ANISOTROPIC NATURE OF RADIALLY STRAINED METAL TUBES

Julie N. Strickland

Thesis Prepared for the Degree of

Master of Science

University of North Texas

December 2015

APPROVED:

Marcus L. Young, Major Professor

Narendra Dahotre, Committee Member
Sundeep Mukherjee, Committee Member
Rajiv Mishra, Committee Member
Nigel Shepherd, Chair of the Department of Material Science and Engineering
Kuruvilla John, Associate Dean of Research and Graduate Studies

Strickland, Julie N. *Anisotropic Nature of Radially Strained Metal Tubes*. Master of Science (Materials Science and Engineering), December 2015, 72 pp., 8 tables, 63 illustrations, references, 28 titles.

Metal pipes are sometimes swaged by a metal cone to enlarge them, which increases the strain in the material. The amount of strain is important because it affects the burst and collapse strength. Burst strength is the amount of internal pressure that a pipe can withstand before failure, while collapse strength is the amount of external pressure that a pipe can withstand before failure. If the burst or collapse strengths are exceeded, the pipe may fracture, causing critical failure. Such an event could cost the owners and their customers millions of dollars in clean up, repair, and lost time, in addition to the potential environmental damage. Therefore, a reliable way of estimating the burst and collapse strength of strained pipe is desired and valuable.

The sponsor currently rates strained pipes using the properties of raw steel, because those properties are easily measured (for example, yield strength). In the past, the engineers assumed that the metal would be work-hardened when swaged, so that yield strength would increase. However, swaging introduces anisotropic strain, which may decrease the yield strength.

This study measured the yield strength of strained material in the transverse and axial direction and compared them to raw material, to determine the amount of anisotropy. This information will be used to more accurately determine burst and collapse ratings for strained pipes. More accurate ratings mean safer products, which will minimize risk for the sponsor's customers.

Since the strained metal has a higher yield strength than the raw material, using

the raw yield strength to calculate burst and collapse ratings is a conservative method. The metal has even higher yield strength after strain aging, which indicates that the stresses are relieved. Even with the 12% anisotropy in the strained and 9% anisotropy in the strain aged specimens, the raw yield strengths are lower and therefore more conservative. I recommend that the sponsor continue using the raw yield strength to calculate these ratings.

I set out to characterize the anisotropic nature of swaged metal. As expected, the tensile tests showed a difference between the axial and transverse tensile strength. The correlation was 12% difference in yield strength in the axial and transverse directions for strained material and 9% in strained and aged material. This means that the strength of the metal in the hoop (transverse) direction is approximately 10% stronger than in the axial direction, because the metal was work hardened during the swaging process. Therefore, the metal is more likely to fail in axial tension than in burst or collapse.

I presented the findings from the microstructure examination, standard tensile tests, and SEM data. All of this data supported the findings of the mini-tensile tests. This information will help engineers set burst and collapse ratings and allow material scientists to predict the anisotropic characteristics of swaged steel tubes.

ACKNOWLEDGEMENTS

Thank you to Dr. Marcus L. Young, my advisor. I appreciate the insightful reviews and the guidance. Brandon Ohl, undergraduate, was my lab assistant, editor, and right-hand man.

Thank you to the sponsor who funded and supported this research. Several people provided valuable technical guidance, asked the important questions, and provided much appreciated technical assistance.

Great appreciation goes to Dr. Rajiv Mishra for unlimited use of his lab and assistance by his graduate students, including Nelson Martinez, Aniket AK.Dutt, and Mageshwari “Maggie” Komarasamy.

Thanks to Stephanie Routh (undergraduate), Michelle Gilbert (undergraduate), Ying Qui (graduate), and Matthew Carl (graduate). My sincere appreciation goes to the Materials Science Department, including all the teachers and other students who assisted us in small but much appreciated ways.

Last but not least, I would like to offer a special thank you to my children, Julian and Emily Strickland, for their loving support and encouragement.

TABLE OF CONTENTS

Page

LIST OF TABLES

Table Page

LIST OF FIGURES

LIST OF ABBREVIATIONS

ASM – American Society for Metals

ASTM – American Society for Testing and Materials

CNC – computer numerical control

EDM – electrical discharge machine

ID – Inner diameter

in – inch(es)

mm – millimeter(s)

MTR – Material Test Report: the document that accompanies the metal tubes from the manufacturer.

OD – Outer Diameter

SEM – scanning electron microscope

Standard Tensile Specimen: per ASTM A370 E8, 2-inch gage section, 0.5" diameter.

UNT – The University of North Texas

UTS – Ultimate Tensile Strength

YS – Yield Strength

1. INTRODUCTION

1.1. Statement of the Problem

Metal pipes are sometimes swaged by a metal cone to enlarge them, which increases the strain in the material. The amount of strain is important because it affects the burst and collapse strength. Burst strength is the amount of *internal* pressure that a pipe can withstand before failure, while collapse strength is the amount of *external* pressure that a pipe can withstand before failure (Jin, 2012; Zhu, 2006; Zhu, 2012). If the burst or collapse strengths are exceeded, the pipe may fracture, causing critical failure (Jin, 2012; Zhu, 2006; Zhu, 2012). Such an event could cost the owners and their customers millions of dollars in clean up, repair, and lost time, in addition to the potential loss-of-life and environmental damage (Busenberg, 2011; Kurtz, 2011). Therefore, a reliable way of estimating the burst and collapse strength of strained pipe is desired and valuable.

1.2. Purpose of the Study

The sponsor currently rates strained pipes using the properties of raw steel, because those properties are easily measured (for example, yield strength). In the past, the engineers assumed that the metal would be work-hardened when swaged, so that yield strength would increase. However, swaging introduces anisotropic strain, which may decrease the yield strength (Mack, 2000).

The purpose of this study is to better understand failure in unstrained, strained, and strained and aged steel tubes by examining the anisotropic effects in the transverse and axial directions through mini-tensile testing. A comparison of the microstructure

and yield strength in these different conditions will be used to more accurately determine burst and collapse ratings for strained pipes. More accurate ratings mean safer products, which will minimize risk for the sponsor's customers.

1.3. Research Objectives

The first research objective involves developing a standard practice for determining yield strength of steel tubes through mini-tensile testing. While strain in tubes can be difficult to test directly, tensile strength can be easily measured and compared. Thus, a method for testing the yield strength in the tube walls needed to be developed. Since the walls were less than 0.5" thick (see section 1.6), traditional dogbone tensile bars could not be cut from the metal (ASTM, 2012). Therefore, mini-tensile tests were employed (see section 2.2 for historical background and section 4 for specimen dimensions and test detail). Different methods of sample preparation were compared, including electropolishing, mechanical polishing with a Dremel tool, and hand polishing, to determine the best method.

Baseline mini-tensile tests were performed on pre-strained (raw) material and compared to standard tensile tests data to validate the testing. Mini-tensile samples were prepared via CNC and from EDM to determine which would correlate best to the standard dogbone. Once the mini-tensile test procedure was validated, the second research objective, which involves comparing the results from mini-tensile testing from four orientations within the tube, was initiated to determine the effect of anisotropy on mechanical behavior in the metal.

1.4. Assumptions

Metal tubes may be strained at different percentages, as a function of the desired ID and OD. The details of pipe manufacturing and applications are outside the scope of this paper, however many variables dictate the choice of ID, OD, and amount of strain, including raw material dimensions, desired dimensions, and cone size. Over the product line, 9.6% was the max strain for pipes less than 22" OD. Therefore, 10% strain was chosen for this project. Similarly, the smallest size, and therefore the weakest, was chosen as a worst case scenario. The pipes are machined as shown in Figure 1.1. The sponsor required the dimensions be deleted from this figure, however, the difference in relative thickness between the thickness of the tubes is evident.

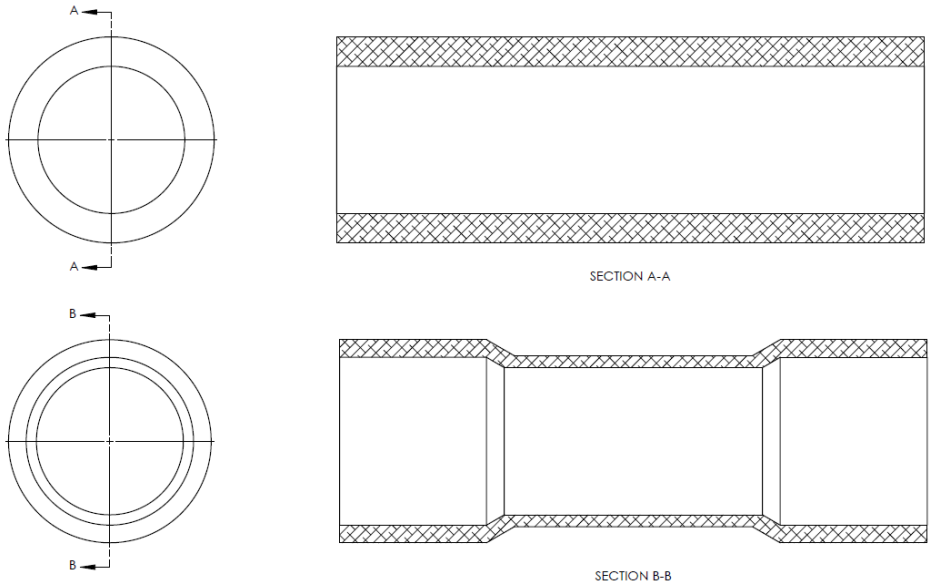

Figure 1.1 Metal Tube Profile Before and After Machining

The material is assumed to be anisotropic due to the processing methods to produce steel tubes. That is, I hypothesized that there would be a measurable difference in tensile strength in the transverse direction compared to the axial direction.

1.5. Rationales

The sponsor requested that mild steel be used in this study because it is increasingly requested by the sponsor's customers. The steel is modified 4140, which includes the elements chrome, molybdenum, sulfur, and boron (ASM, 1990). Chrome and molybdenum increase corrosion resistance and strength (ASM, 1990). The amount of carbon is controlled to determine the amount of martensite, which greatly affects the material properties (ASM, 1990). Sulfur increases machinability, but decreases corrosion resistance, so the amount is kept low (ASM, 1990). Boron increases the hardenability (ASM, 1990).

1.6. Research Methods

The material examined in this study falls into three categories: 1) raw (as-received or pre-strained), 2) strained, and 3) strained and aged. The "raw" metal is in the as-received condition from the tube manufacturer. It likely contains some strain from the manufacturing process, so a small amount of anisotropy is expected initially. The raw metal is used as a baseline. That is, I measured the properties of the raw metal through standard tensile tests to have an industry-standard-approved set of data for comparison. I then compared the mini-tensile test results of raw metal with the standard tensile test results to validate the test method.

The strained metal results from machining and swaging the raw tubes. These tubes were machined to a wall thickness of less than one-half inch to reduce the amount of force required to strain the metal. Figure 1.1 depicts the as-received and machined tube profiles. The larger diameter is where the cone rests initially and is called the launcher section. After the cone has traveled the length of the tube, the entire tube will be approximately the same outer diameter. Since the thickness of the walls is less than 0.5", standard tensile test specimens cannot be manufactured from this metal for comparison. "Strained and aged" specimens are from tubes that were machined, swaged, and subjected to 350ºF for 18 hours. Section 2.3 explains this in more detail.

Strain in tubes can be difficult to test directly. However, tensile strength is more easily measured and compared, so tensile tests were performed on the metal. Stress is related to strain by

$$\sigma = K\epsilon^n$$

where σ represents the stress and ϵ represents the strain (Jin, 2012). *K* and *n* are constants determined by the stress-strain curve (Jin, 2012). In this case, *K* is the slope of the linear region and is the Young's Modulus, which is a constant for a given material (Jin, 2012). The constant *n* is dependent on the strain rate and is assumed, for simplification, to be equal to one (1). Therefore, by measuring the stress in the metal, we are indirectly measuring the strain.

The microstructure of the samples was examined to understand the effects of the straining and aging processes. Mini-tensile specimens were machined, polished, and tested. The first set of samples was prepared from the raw material with the CNC

machine and the results were compared to those from a similar number of EDM samples. The set of data that most closely correlated to the standard tensile specimens determined the machining method used for the additional samples. Since the CNC method required polishing off the substrate and may result in varying thickness of samples, I hypothesized that the EDM samples would have the closest correlation. The CNC method is explained in greater detail in Section 4 (Figures 4.4, 4.5, and 4.6).

1.7. Naming Convention

The specimens were named as shown in Figure 1.2. The materials are those mentioned previously: raw, strained, and strained and aged. The directions include axial, transverse, and radial as shown in Figure 1.3. The location is only applicable to the raw material, which is thick enough to have specimens made in the inner and outer diameter locations. The exception is the "Through" direction, which applies to the "Strained" and "Strained and Aged" material. Each group of unique letters constitutes a series, which are grouped together on graphs and in the tables. The specimen number is a consecutive number from 1 to 15, depending on how many specimens were tested.

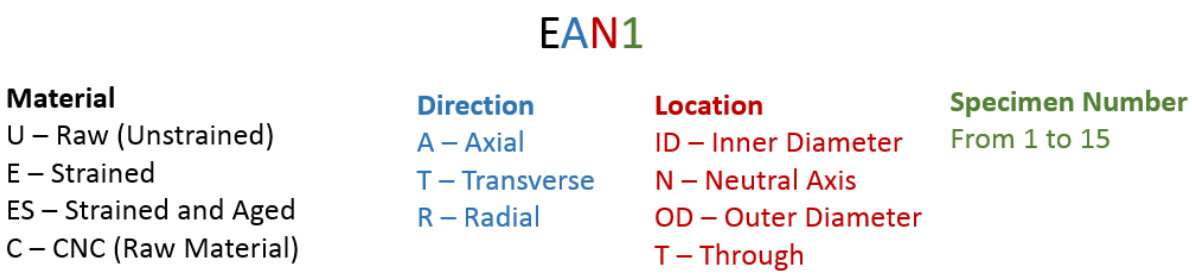

Figure 1.2 Specimen Naming Convention

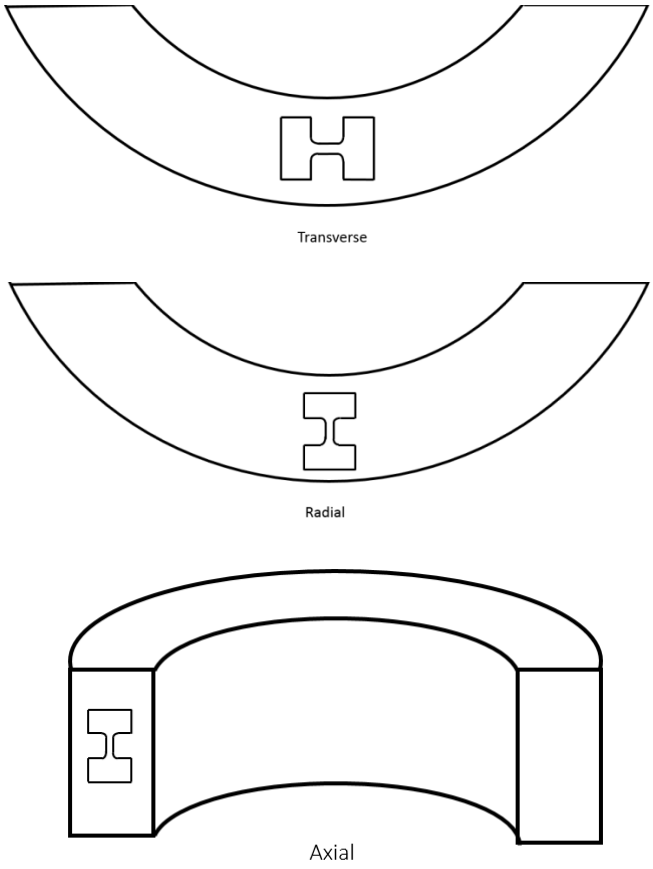

Figure 1.3 Directions of Specimens in the Metal Tube

1.8. Limitations

Surface scratches or burrs may serve as crack propagation sites and skew the results. I polished the specimens on 1200 grit polishing pads to minimize those effects. However, the sides were not polished. The irregularities on the recast surface were potential sites for crack propagation and may have resulted in lower yield strength values. To evaluate this and other variables, the mini-tensile test data was compared to full-sized tensile test specimens. Also, SEM images of the fracture surface were examined to determine the origin of the failure and failure mode (Section 5).

Similarly, the radius where the gage section meets the wider grip section on the mini-tensile specimen was predicted to be a stress concentration point. This theory was disproven, since the specimens broke in the middle of the gage section as desired (Figure 4.17).

Prior to starting this project, a customer noted that EDM may cause hydrogen embrittlement, which is explored in Section 2.5.

Various polishing methods were explored, including chemical and electrochemical methods. Specimens were dipped and soaked in sulfuric acid, phosphoric acid, hydrochloric acid, or aqua regia for varying times. The chemical solutions, times, and voltages were chosen from a reference handbook (American Society for Metals (ASM), 1964; ASM, 1973; Latifi, 2013; ASTM, 2009). The solutions had either no effect or deposits formed on the surface. Electrochemical polishing was not effective for this metal.

Mechanical polishing using a polishing wheel was not performed due to the difficulties associated with securing the mini-tensile specimens during polishing. It would have been possible to mount and polish the mini-tensile specimens, but this was not performed due to difficulties associated with removing the substrate (Bakelite or phenolic material) after polishing. A Dremel® tool was recommended and tried. The Dremel® attachment was too large to fit into the corner of the specimen and simply polished a small portion of the side. The Dremel® tool's felt attachment removed some of the recast layer but not all. The other polishing attachments may have introduced surface scratches; the grit number was not listed. Therefore, it was determined that

polishing the specimens manually using polishing pads was the best method for removing the recast layer.

1.9. Summary

I prepared mini-tensile specimens from mild metal using EDM and CNC machines. After comparing the results to the full-sized tensile test specimens, I prepared additional samples. The test procedure was fully documented in text and images. The time from polishing to testing was minimized to eliminate concerns about hydrogen embrittlement. By comparing the transverse and axial properties, the effect of anisotropy on mechanical properties of the steel pipes was quantified. Engineers can use this information to set burst and collapse ratings on strained pipes in the future, to ensure a safer product line and minimize customers' risk.

2. RELATED LITERATURE

2.1. Introduction

Mini-tensile testing has been used to determine material properties for well over a decade. In this study, mini-tensile testing was performed to determine the yield strength in various directions of a steel tube. Expected results based on past research are discussed below, along with industry standards.

2.2. Historical Background

Mini-Tensile Tests

Mini-tensile testing using our particular experimental setup has been performed as early as 2000, when researchers from the University of Missouri, University of California, and Rockwell Science Center tested friction stir welded aluminum alloys (Mishra, 2000). Before using mini-tensile testing, it is important understand the Scaling Effect, which correlates the material properties of the mini-tensile specimens with the full-sized specimens (Sergueeva, 2009). The “scaling effect” includes the effects of specimen size, geometry, grain size, anisotropy, surface effects, and residual stress (Sergueeva, 2009). It was found that the yield stress and ultimate tensile strength (UTS) were not noticeably affected by gage length, while Young modulus values increase with gage length (Sergueeva, 2009).

Effect of Strain on Steel Tubes

Centro Sviluppo Materiali S.p.A. (an Italian lab) found that the estimated post-strained tensile yield stress for strained low alloy steel was 147 ksi (1013 MPa). The same report stated that previous tests had values within 10% of this value (132 to 159

ksi) (Bufalini, 2010). However, Shell E&P Technology Applications and Research and Enventure Global Technology showed that low alloy steels showed an increase whereas higher strength metals showed a decrease in yield strength (Mack, 2000). L-80 was in the middle and showed little change, and since the steel tested has a higher yield strength than L-80 (110 versus 80 ksi), an increase in yield strength is expected (Mack, 2000).

Bauschinger Effect

Especially pertinent to thick-walled tubes, the Bauschinger Effect explains that some metals experience lower yield strength after being loaded in the reverse direction (Huang, 2006; Li, 1977). "Thick-walled" is typically accepted as having a diameter to thickness ratio of less than 10. The equations below show that the tubes discussed herein are thin-walled tubes (d/t >10), and therefore, the Bauschinger Effect does not apply.

One method to reduce the Bauschinger Effect in steels is by dynamic strain aging, which is defined as applying a constant strain for some specified time at temperatures between 250 to 450ºF (Latifi, 2013 and Mack, 2003). Therefore, even if the thickness ratio is ignored, the Bauschinger Effect is small or absent.

2.3. Industry Standards

Specimen Size

ASTM A370, section A2.2.4.3, states, "Small-size specimens proportional to standard…may be used when it is necessary to test material from which the standard specimen cannot be prepared. Other sizes of small-size specimens may be used. In

any such small-size specimen, it is important that the gage length for measurement of elongation be four times the diameter of the specimen. The elongation requirements for the round specimen 2-inch gage length in the product specification shall apply to the small-size specimens" (ASTM, 2012).

So in our case:

$$4\mathrm{d} = 4 * (1\ \mathrm{mm}) = 4\ \mathrm{mm}$$

The specimens used have 2 mm length gage sections, which do not meet this note for round specimens. However, the specimens are not round. As stated previously, that gage length does not noticeably affect yield strength. Since the wall thickness of the smallest tube is less than half an inch and the transverse properties must be measured as well, the largest mini-tensile sample was limited. This is covered by the first sentence in the quote above, "…when it is necessary to test material from which the standard specification cannot be prepared" (ASTM, 2012).

Aging

Section 9.4 of ASTM A370 allows for aging of specimens for less than 48 hours by heating in an oven and other methods (ASTM, 2012). Previous researchers aged steel at 175ºC (347ºF) for five hours (Mack, 2002). "The time and temperature were selected based upon a study of the kinetics of strain aging for these products and are a realistic simulation of response of these materials in downhole conditions," according to Robert Mack (2002). The sponsor used 177ºC (350ºF) at 18 hours, which is approximately the same temperature for a longer duration. This method of aging simulates fast-forwarding the clock 10 years; that is, the material properties are

assumed to be equal to a 10-year-old specimen. The sponsor calls this “strain aging,” so that term will be used in this paper.

2.4. Hydrogen Embrittlement

Hydrogen embrittlement is a broad term which refers to a wide variety of failure mechanisms which result from the formation of embrittling hydrides and lead to a lower yield strength (Bernstein, 1986). Well-tempered steel with a martensitic structure are more hydrogen-resistant (Bernstein, 1986). Also, higher strength metals are more susceptible; steels with strengths below 102 ksi show no significant embrittlement (Bernstein, 1986). The steel is martensitic, but its 110 ksi yield strength is just about the threshold for susceptibility of hydrogen embrittlement. Since susceptibility increases with yield strength (Bernstein, 1986), the chances for hydrogen embrittlement of the steel are low.

2.5. Summary

Mini-tensile testing using our specific setup has been used to determine material properties for well over a decade. In our study, mini-tensile testing was performed to determine the yield strength in four directions of an strained tube. The Bauschinger Effect is not applicable here because the tubes are thin-walled. Chances for hydrogen embrittlement are low.

3. MICROSTRUCTURES

As shown in Figure 3.1, the microstructure of the raw material consists of predominantly martensite, as expected, with a small amount of proeutectoid ferrite and and compared nicely to that found for 4140 steel tube (Figure 3.2) in the ASM Specialty Metals Handbook. Hardness values for the sample also match the handbook's values for martensite (Figures 3.3 and 3.4).

Figure 3.1 Raw Material, Top View of Tube, 1000X

Figure 3.2 Microstructure of 4140 Steel Tube (ASM, 1973), which has been austenitized at 830 C for 1 hour, oil quenched, tempered at 595 C for 2 hours. The white objects are proeutectoid ferrite and black objects are martensite.

Table 1 Effect of carbon concentration and percentage martensite on the as-quenched hardness of steel

Carbon, %	Hardness, HRC				
	99% M	95% M	90% M	80% M	50% M
0.10	38.5	32.9	30.7	27.8	26.2
0.12	39.5	34.5	32.3	29.3	27.3
0.14	40.6	36.1	33.9	30.8	28.4
0.16	41.8	37.6	35.3	32.3	29.5
0.18	42.9	39.1	36.8	33.7	30.7
0.20	44.2	40.5	38.2	35.0	31.8
0.22	45.4	41.9	39.6	36.3	33.0
0.24	46.6	43.2	40.9	37.6	34.2
0.26	47.9	44.5	42.2	38.8	35.3
0.28	49.1	45.8	43.4	40.0	36.4
0.30	50.3	47.0	44.6	41.2	37.5
0.32	51.5	48.2	45.8	42.3	38.5
0.34	52.7	49.3	46.9	43.4	39.5
0.36	53.9	50.4	47.9	44.4	40.5
0.38	55.0	51.4	49.0	45.4	41.5
0.40	56.1	52.4	50.0	46.4	42.4
0.42	57.1	53.4	50.9	47.3	43.4
0.44	58.1	54.3	51.8	48.2	44.3
0.46	59.1	55.2	52.7	49.0	45.1
0.48	60.0	56.0	53.5	49.8	46.0
0.50	60.9	56.8	54.3	50.6	46.8
0.52	61.7	57.5	55.0	51.3	47.7
0.54	62.5	58.2	55.7	52.0	48.5
0.56	63.2	58.9	56.3	52.6	49.3
0.58	63.8	59.5	57.0	53.2	50.0
0.60	64.3	60.0	57.5	53.8	50.7

M, martensite

Figure 3.3 Martensite Hardness Values, Table (ASM, 1973)

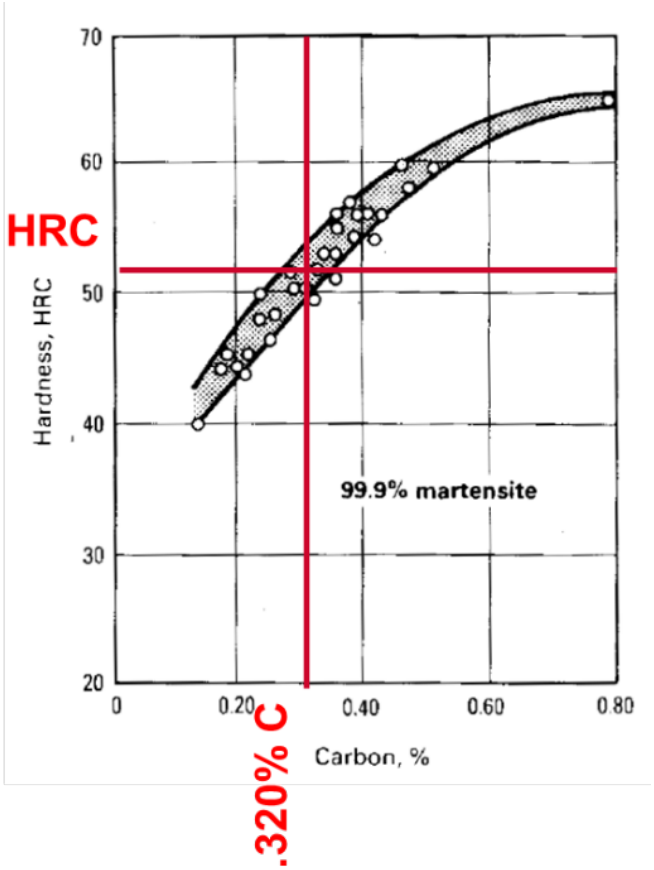

Figure 3.4 Martensite Hardness Values, Graph (ASM, 1973)

Figures 3.5 and 3.6 show side-by-side comparisons of optical microscope images of the microstructure at 100X and 500X magnification, respectively. No significant difference is observable in the raw, strained, and strained and aged specimens. The axial (side) and transverse (top) views are shown.

Axial or Transverse	Raw	Strained	Strained and Aged
Axial (Side)	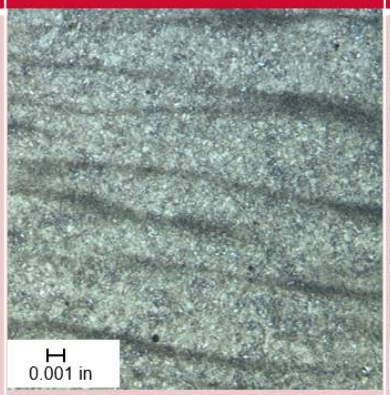	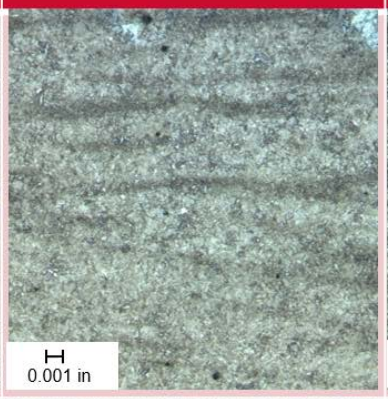	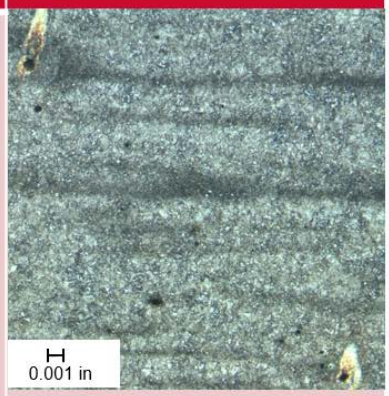
Transverse (Top)	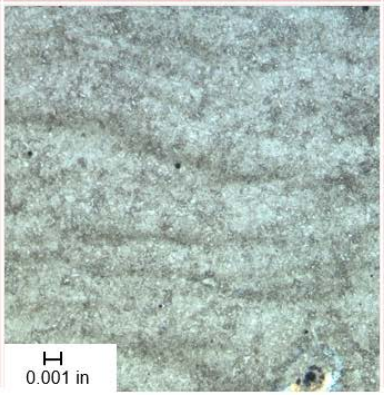	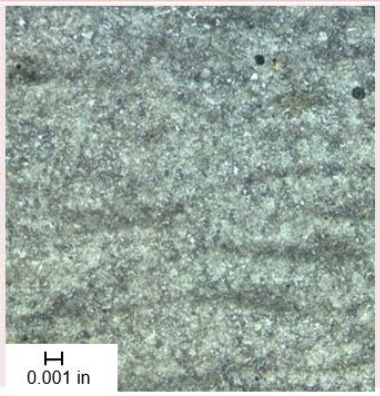	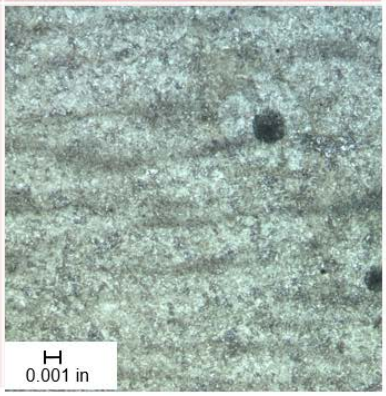

Figure 3.5 Optical Microscope Pictures 100X

Figure 3.6 Optical Microscope Pictures 500X

The stripe-like dark bands in Figures 3.5 and 3.6 on the metal are composed of manganese which were segregated during solidification (Caballero, 2006; Herring, 2013). Thermal treatments and slower cooling rates can minimize or eliminate such bands, but the fast cooling (quenching) is necessary to obtain martensite (Caballero, 2006; Herring, 2013). Per the MTR, the metal tested was quenched twice (though the details of the proprietary treatment were not disclosed).

The sponsor performed micro-hardness tests on the bands to determine if the lighter areas were harder or softer than the darker areas (e.g. the manganese bands).

The data is shown in Table 3.1. The difference between the substrate and bands was not significant. It was less than 2.2 HRC.

Table 3.1 Micro-Hardness Values

Test	Point	Distance	HRC	Comment
1	1	0.000	31.6	Dark
1	2	0.000	30.9	Light
1	3	0.000	32.3	Dark
1	4	0.000	30.1	Light
2	1	0.000	30.9	Transverse
2	2	0.005	30.1	Transverse
2	3	0.010	31.2	Transverse
2	4	0.015	30.9	Transverse
2	5	0.020	31.2	Transverse
2	6	0.025	30.9	Transverse
2	7	0.030	30.1	Transverse
2	8	0.035	32.3	Transverse
2	9	0.040	29.6	Transverse
2	10	0.045	30.5	Transverse
2	11	0.050	30.5	Transverse
2	12	0.055	30.9	Transverse
2	13	0.060	30.5	Transverse
2	14	0.065	30.5	Transverse
2	15	0.070	32.0	Transverse
2	16	0.075	30.1	Transverse
2	17	0.080	29.6	Transverse
2	18	0.085	30.5	Transverse
2	19	0.090	32.3	Transverse
2	20	0.095	29.2	Transverse
2	21	0.100	30.1	Transverse
			30.8	**Average**
			0.8	**Std Dev**

4. MINI-TENSILE SPECIMENS

4.1. Sample Preparation

Three quantity CNC and 5 EDM mini-tensile specimens were prepared per the drawing in Figure 4.1, with a thickness of 1 millimeter (mm). Since CNC is a drilling process, there was a possibility that the micro-structure of the specimen would be changed by work hardening or heat effects. Similarly, the EDM process uses voltage across a wire, submerged in water, so hydrogen embrittlement may have developed (Section 2.4). Therefore, the specimens were prepared, tested, and the results compared, to determine which correlated the most closely to the standard tensile test results.

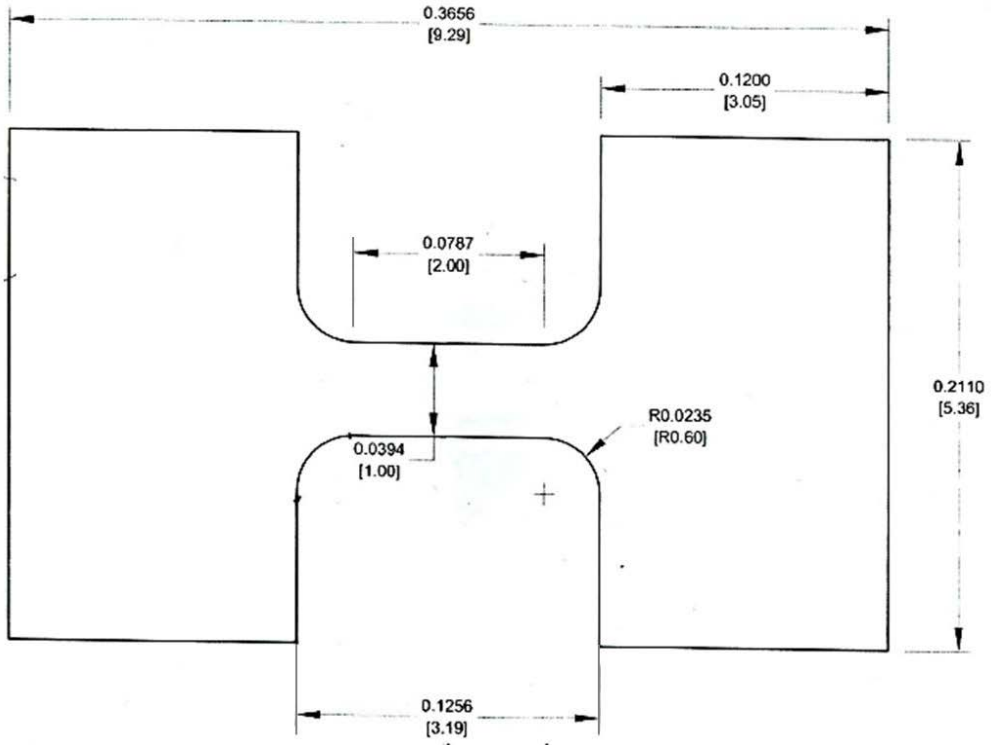

Figure 4.1 Mini-tensile Specimen Dimensions, inches [mm]

Figure 4.2 shows a typical EDM machine with computer controls. This machine is in a lab at UNT, while our samples were prepared by Applegate EDM (an outside lab) and the sponsor's machinists. This distinction is important because the exact machine plays a role in the later discussion on recast layers. A typical EDM specimen is depicted in Figure 4.3.

Figure 4.2 EDM Machine

Figure 4.3 EDM Specimen

Figure 4.4 depicts the CNC machine at UNT used to create the samples. Note that the CNC uses a 0.1-inch drill bit and 0.01 inch/minute feed rate. This very small bit and very slow rate minimize the surface effects of the machining operation. The CNC drills down 1 mm into a 2 mm thick sheet of metal (Figure 4.5). The remaining 1 mm is polished off; this operation was performed in the sponsor's lab. The resulting specimen has burrs and rough edges (Figure 4.6).

Figure 4.4 CNC Machine at UNT

Figure 4.5 Sample 1-1 CNC

Figure 4.6 CNC Specimen (See Figure 4.1 for dimension)

Figure 4.7 depicts the CNC transverse neutral (CTN) series and the raw, EDM, transverse (UTN) specimen. There is a strong correlation; the curves overlap

beautifully. From this, I inferred that the machining methods were equally good. Since EDM is less time-intensive and the results were comparable, EDM was used to make subsequent specimens.

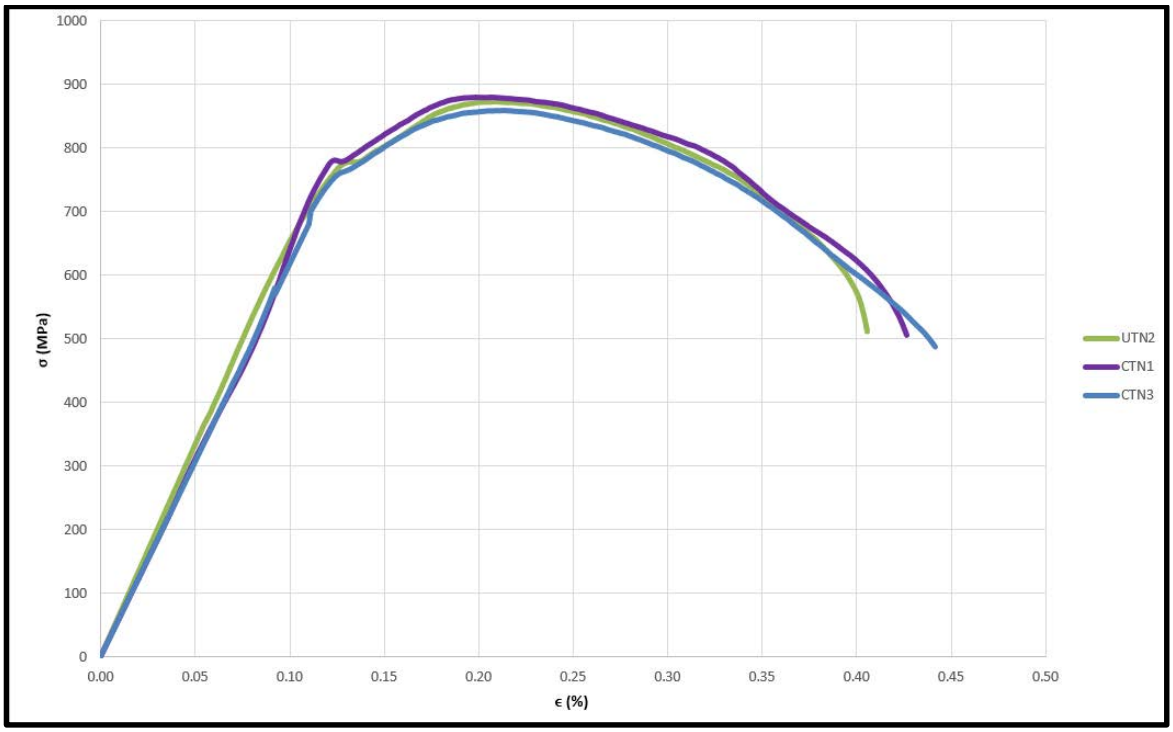

Figure 4.7 Raw CNC Transverse Neutral (CTN) and Raw EDM Transverse Neutral (UTN) Graph

Mini-tensile specimens were prepared from various locations and directions in the tube (Figures 4.8, 4.9, and 4.10). The goal was to measure and compare the yield strength at these various locations to determine the amount of anisotropy in the metal. The raw metal was tested as a baseline. The results from the raw axial specimens were compared to the full-sized tensile test results, which were also in the axial direction. After this baseline was established correlating the mini-tensile to full-sized tensile test results, further tests were performed. The transverse and radial directions

on the neutral axis were tested for comparison. Inner diameter, outer diameter, and neutral axis were compared using the through-wall specimens. That is, metal was cut all the way through the wall of the tubes and then sliced into as many specimens as possible (Figure 4.8). The differing yield strengths reflected the different stresses through the wall of the strained and strained and aged tubes. Through-wall specimens were taken in the axial and transverse directions. (The curved surfaces through the walls of the tube in Figure 4.8 are the result of machining the full sized tensile specimens which are used as a baseline.)

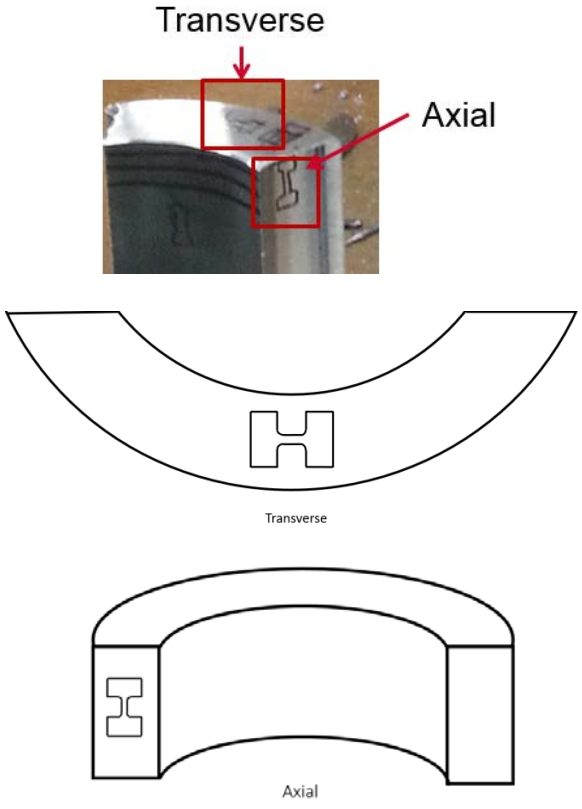

Figure 4.8 Transverse and Axial Directions

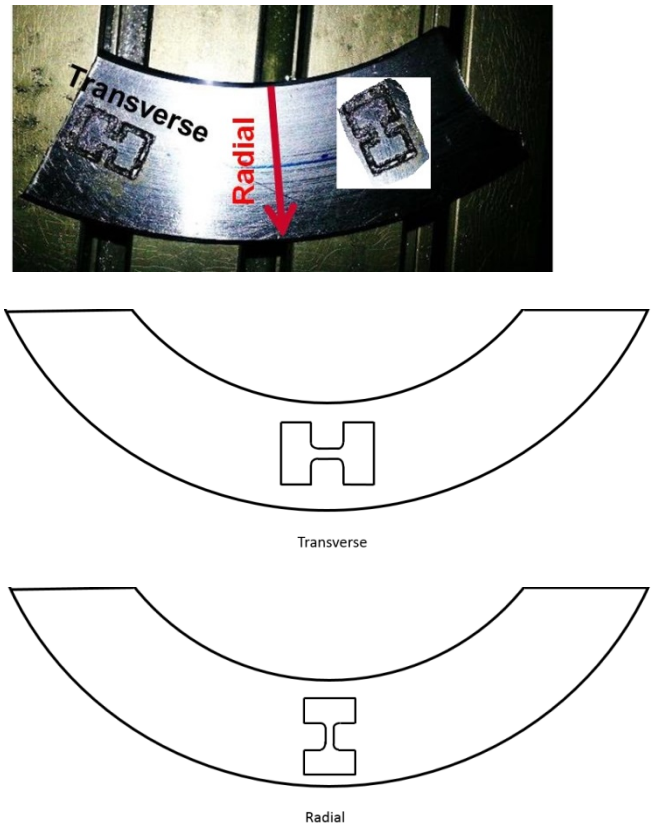

Figure 4.9 Transverse (Neutral Axis) and Radial Directions

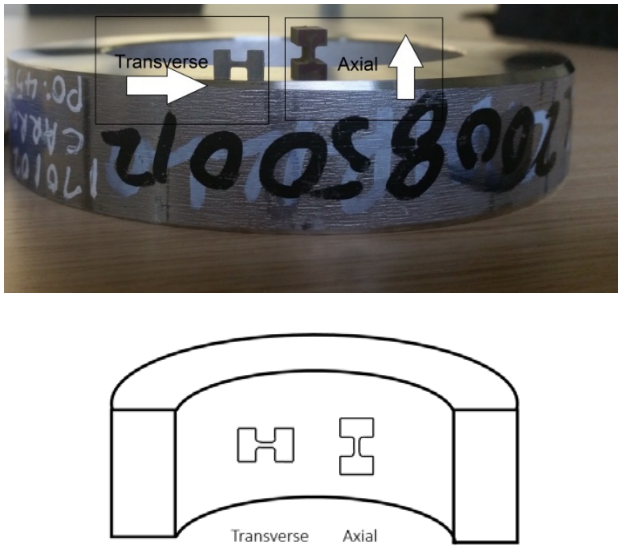

Figure 4.10 Transverse and Axial Direction for Through the Wall Specimens

After the samples were machined by either CNC or EDM, the specimens were polished using 1200 grit polishing pads to remove the recast layer. Polishing was performed by placing the mini-tensile sample flat on the polishing pad and moving it in circles manually. Therefore, the narrow sides of the specimen were not polished and still have the recast layer. The samples were then cleaned in methanol. The interval between polishing and testing was less than an hour to reduce the amount of oxidation. A typical polished mini-tensile sample is shown in Figure 4.11. According to the ASM Handbook, mechanical polishing at room temperature affects the material to a depth less than 0.050 mm (0.002 in) (ASM, 1994).

Figure 4.11 Typical Polished Mini-Tensile Specimen

Figure 4.12 shows the results of mini-tensile tests performed on various UAN specimens. UAN1 through UAN8 were one of the first sets polished, while UAN11 through UAN15 were performed at the end of the program. As the wide scatter of the first set shows, polishing has a big effect on the results. The latter set has a much tighter grouping, e.g., more precise results.

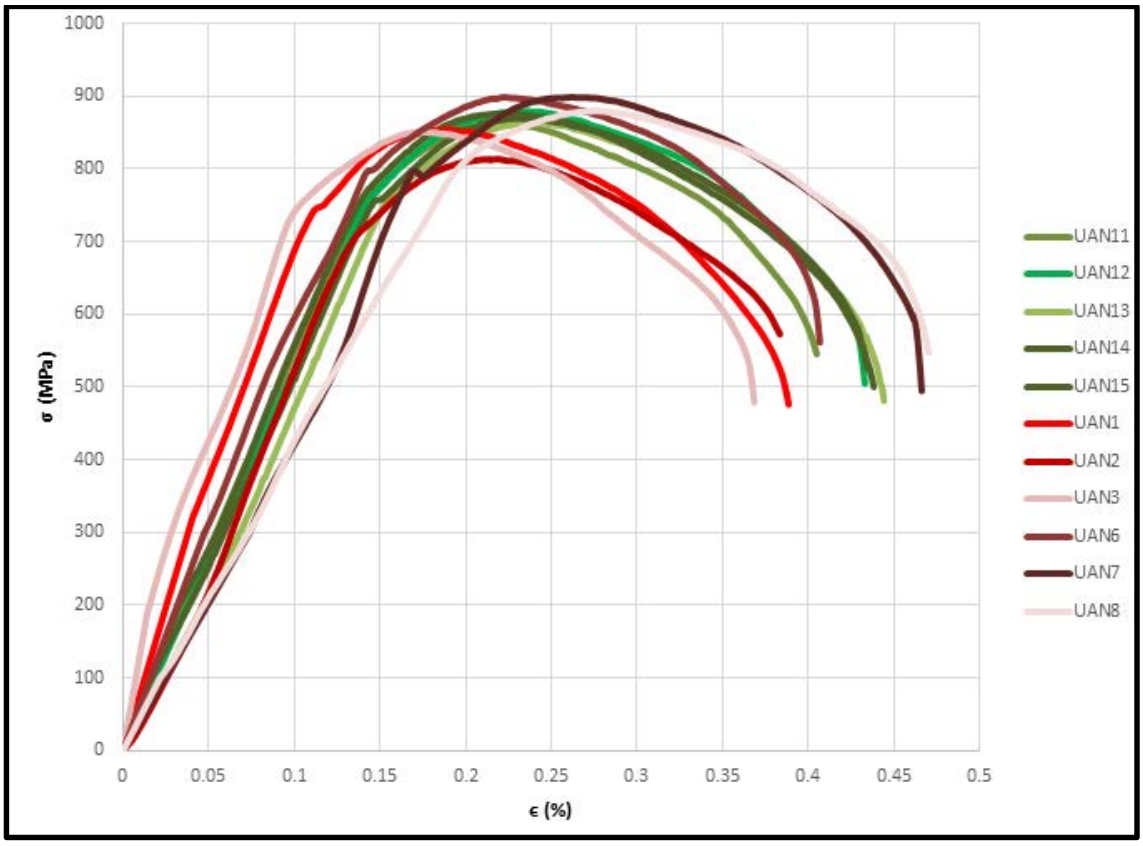

Figure 4.12 The Effect of Polishing on UAN Specimens

4.2. Mini-tensile Test

Figure 4.13 shows the mini-tensile testing machine and Figures 4.14 and 4.15 show details of the grips for mounting the mini-tensile sample. Since standard extensometers cannot measure the small elongation of the sample, the displacement of the crosshead is measured and used to determine the amount of strain. While the mini-tensile testing machine includes a temperature-control enclosure, the mini-tensile testing for this study was performed at room temperature. The data acquisition software and some of the hardware were created by National Instruments.

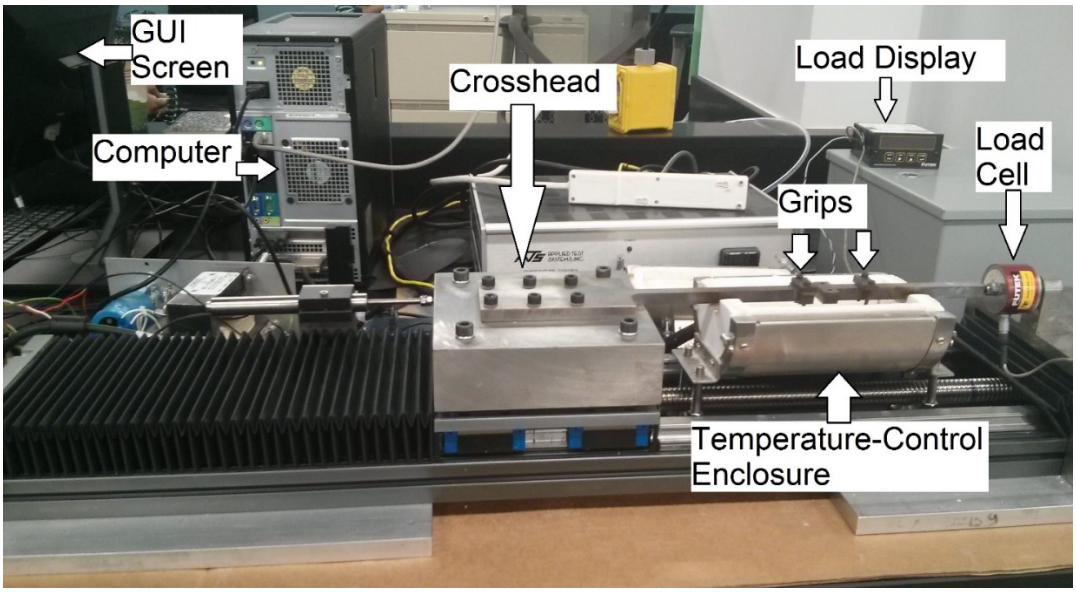

Figure 4.13 Mini-tensile Test Machine

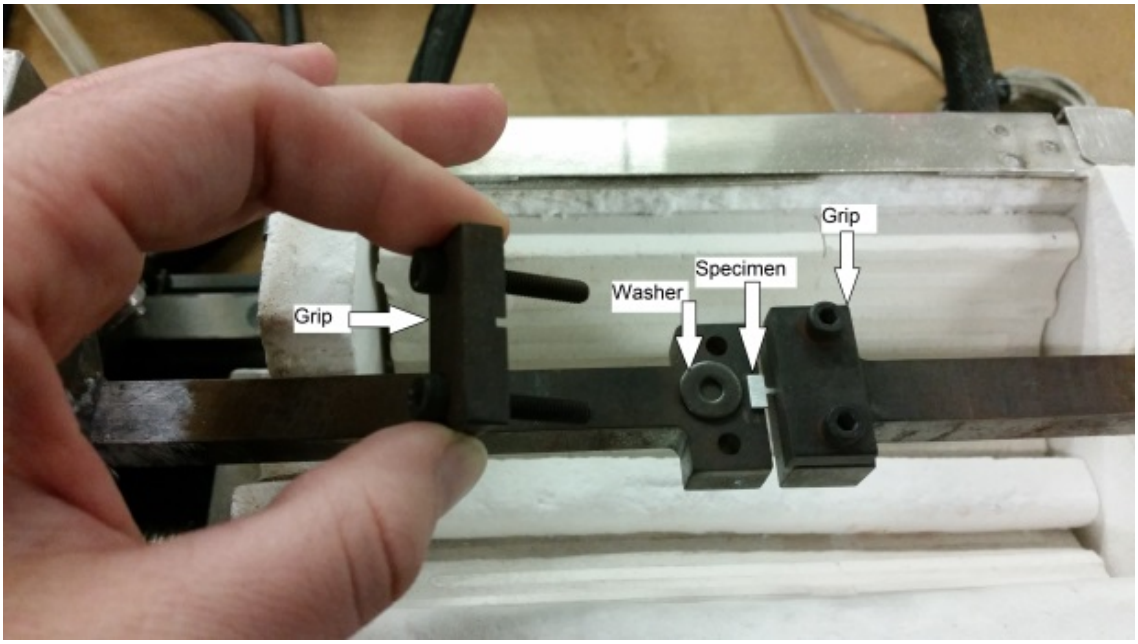

Figure 4.14 Grips and Specimen

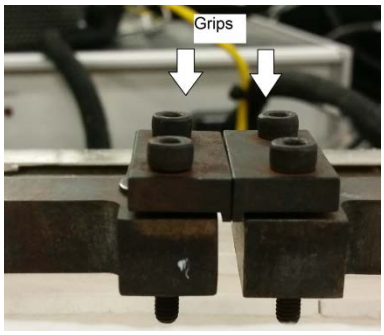

Figure 4.15 Mini-tensile Machine Grips Holding a Sample

The Graphical User Interface (GUI) screen is shown in the Test Set Up (Figure 4.16) and close up (Figure 4.17). Manual cross-head speed is only applicable when the sample is being loaded and the cross-heads are moved by pressing the oval button. Once the test begins, the strain rate listed ("Step-1 strain rate") applies in units of mm/mm-sec, or per second (s^{-1}). The gage length (2 mm), measured width, and measured thickness are entered manually for each specimen.

Figure 4.16 Test Set Up

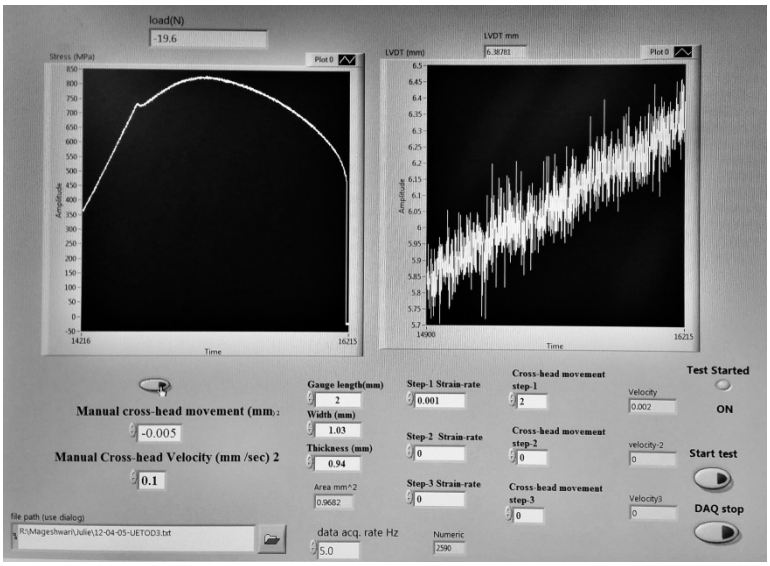

Figure 4.17 Mini-tensile Test Graphical User Interface

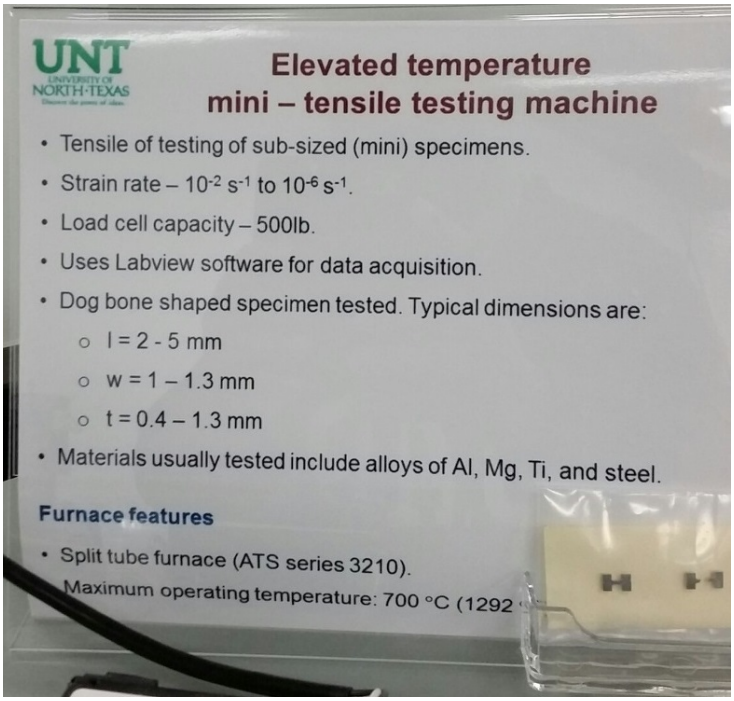

Figure 4.18 Mini-Tensile Test Machine Properties

A typical specimen after fracture is shown in Figure 4.18. The fact that it broke near the center of the gage shows that the radii where the grip section meet the gage

section were not the source of crack propagation. Therefore, these radii are not a significant stress concentration factor.

Figure 4.19 Typical Specimen After Fracture

4.3. Data Analysis

After the tests were complete, the data was analyzed using Origin Pro 8.5.1 software. The process is detailed in Appendix A.

4.4. Summary

Mini-tensile test specimens from various locations and directions in the tubes (raw, strained, strained and aged) were manufactured. EDM and CNC results were compared for two comparable specimens. The other specimens were all created using EDM. The data was analyzed using OriginPro 8.5.1 software. The graphs were used to find the 0.02% Offset Yield Strength, UTS, and percent elongation.

Mini-tensile test results are included in Section 6 and are discussed in Section 7.

5. SCANNING ELECTRON MICROSCOPE

The scanning electron microscope used is a Quanta 200 shown in Figure 5.1. The GUI is shown in Figure 5.2.

Figure 5.1 SEM

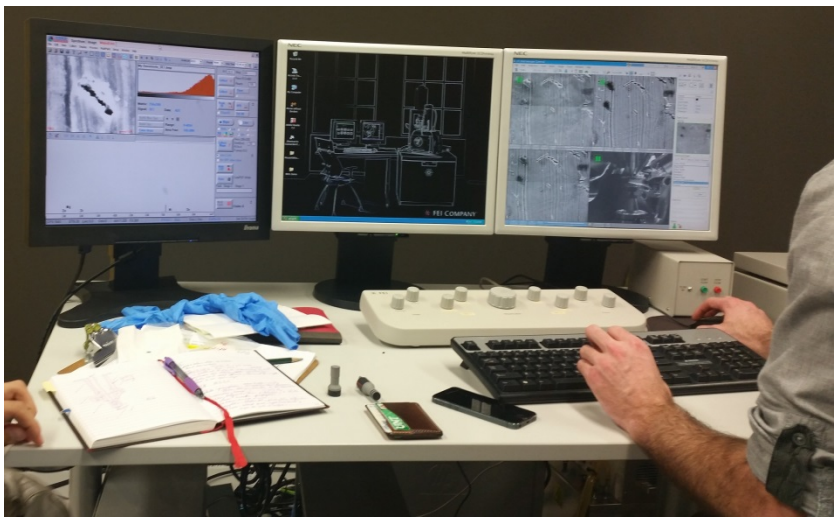

Figure 5.2 SEM GUI

5.1. Recast Layer

Figure 5.3 depicts the recast layer on an EDM specimen manufactured by Applegate EDM. These peaks, spheres, and rough surfaces are typical for EDM (Khanra, 2007; Ramasawmy, 2007; Fukuzawa, 1993). Figure 5.4 shows the recast layer on an EDM specimen manufactured by the sponsor's machinist. Both machines submerged the sample in water, so differences in the recast layers were unexpected. However, Khandra *et al* report that lower EDM energy input resulted in smaller surface structures, while higher energy input resulted in hollow spheres, surface cracks, and other structures (Khandra, 2007). The porous structures contain high percentages of carbon and vary in height from 6.5 to 12.8 micrometers (μm), with an average of 10 μm (Figure 5.5). The recast layer was so thin on the sponsor's specimens that they were not measureable, and are estimated to be 1 μm.

Figure 5.6 shows that these structures are absent after mechanical polishing. Some pitting and fissures are shown on the surface, including some scratches induced by polishing.

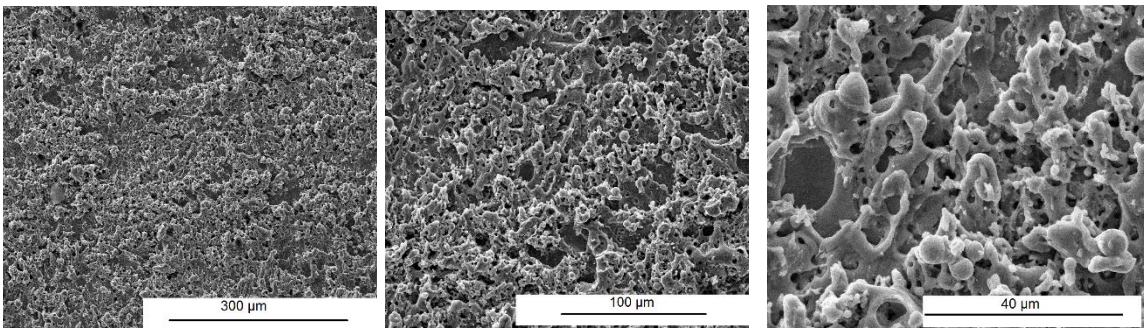

Figure 5.3 SEM Images of the Recast Layer on EDM Specimens from Applegate EDM

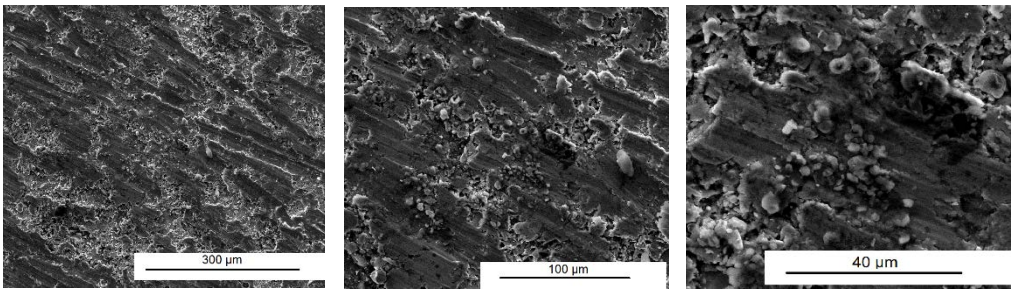

Figure 5.4 SEM Images of the Recast Layer on EDM Specimens from the Sponsor

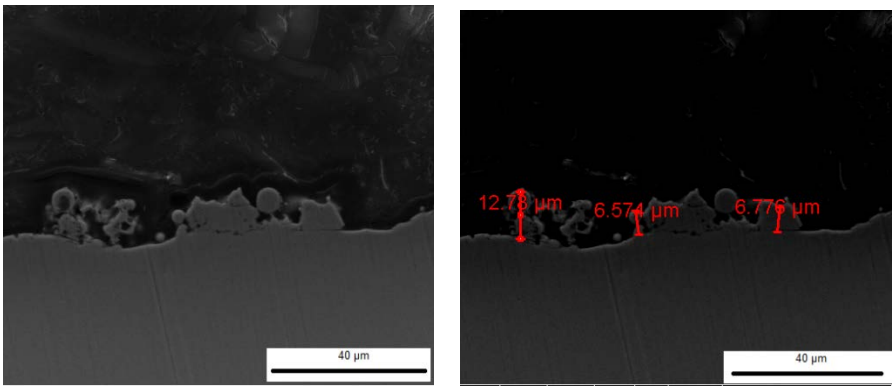

Figure 5.5 Recast Layer Measurements on EDM Specimens from Applegate

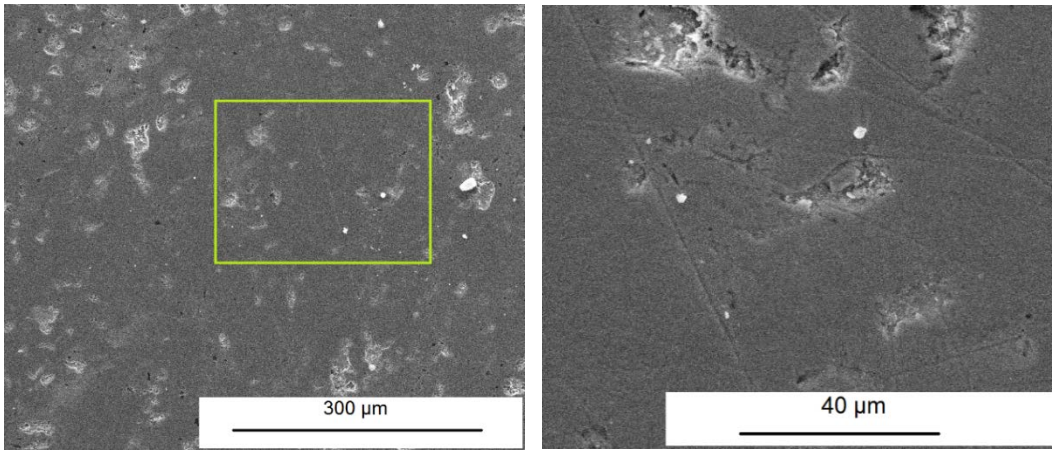

Figure 5.6 SEM Images of Polished Sample ETN1

5.2. Fractured Surface

The fractured surface of the sample ETN1 is shown in Figure 5.7. The ETN series is made from strained material, in the transverse direction, along the neutral axis. This was sample number 1 of the series. The left hand picture shows necking in the middle of the gage section. This is typical of all but a couple of samples, indicating that the radius where the gage section met the grip section did not affect the fracture. That is, the fracture did not commence or propagate from the radius.

The fracture surface of EAN3, the third of the strained axial neutral series, was examined on the SEM. Images of the middle of the fracture show voids where the material failed initially (Figure 5.8). The cup and cone formation at the tip, voids in the middle of the fracture, and the shape of the stress-strain curve indicate ductile fracture (Courtney, 2000). In Figure 5.9, the Elemental Spectrum of the area shows typical mild steel. That is, the voids did not form on a manganese band.

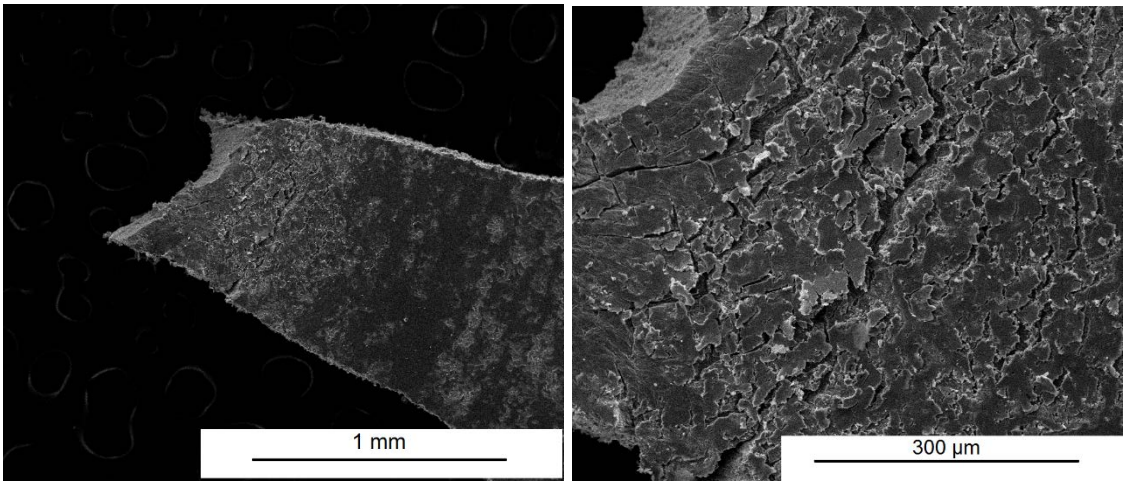

Figure 5.7 SEM Images of the Fractured Surface of Sample Strained Transverse Neutral (ETN1)

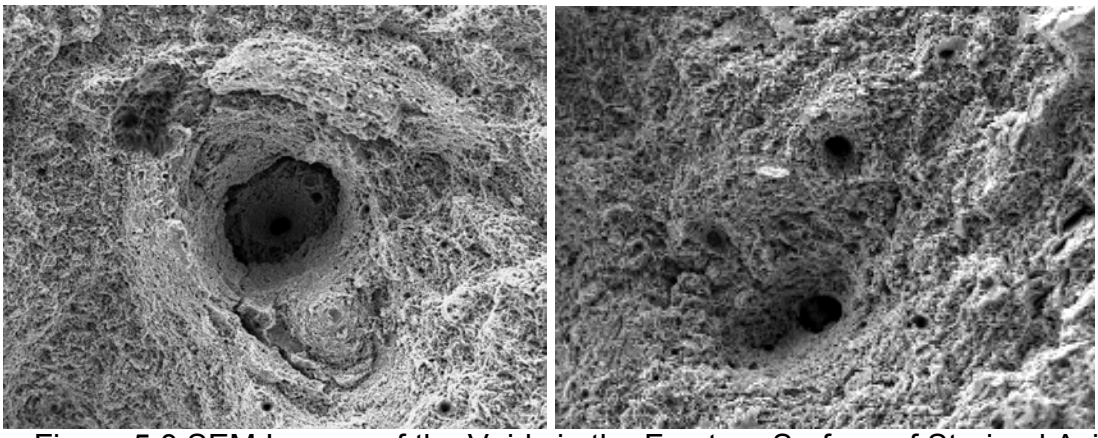

Figure 5.8 SEM Images of the Voids in the Fracture Surface of Strained Axial Neutral (EAN3)

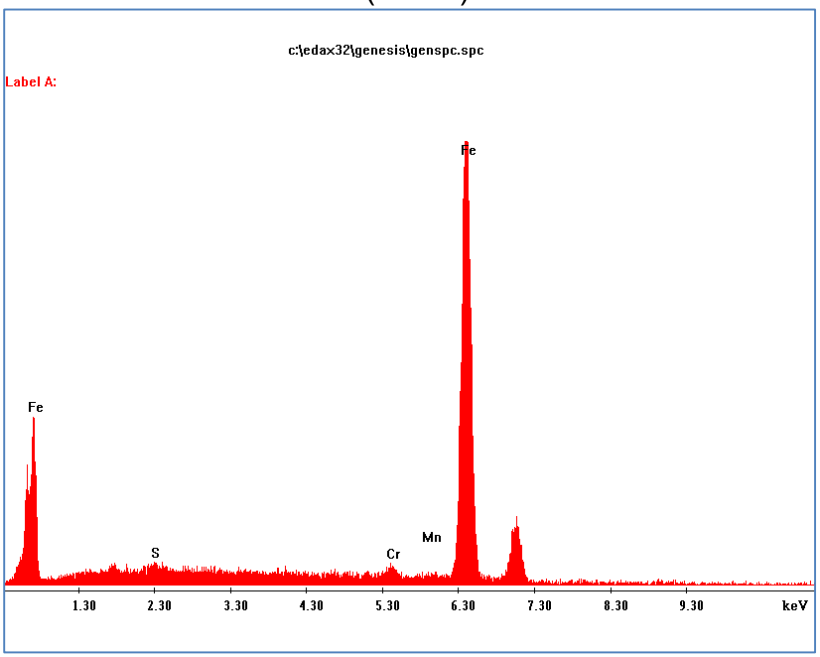

Figure 5.9 Elemental Spectrum of the Area Shown in Figure 5.7

5.3. Elongated Grains

The microstructures of each series were examined using the SEM to determine differences. Long metal tubes that have been swaged shorten approximately 3 inches per 60 inches of tube, so the grains should be wider in the transverse direction than the axial direction. However, since the steel is martensitic, the grains are lens-shaped.

Elongation is obscured by their shape. Figure 5.10 shows martensitic steel, but the change in microstructure was not evident in this image. Compare to Figures 3.5 and 3.6. While circular grains might have elongated to ovals, the martensite has no visual difference from the added strain.

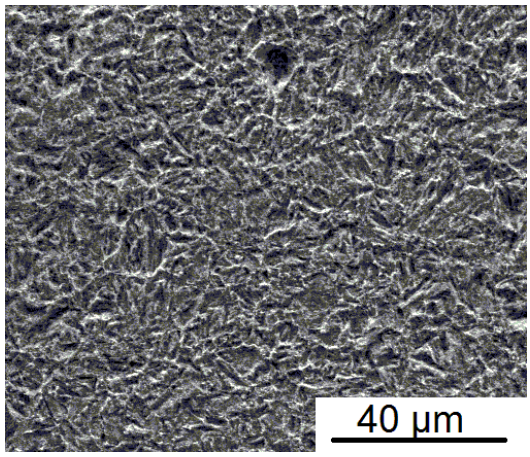

Figure 5.10 SEM Image of the Strained Steel (Top)

6. TENSILE TEST RESULTS

6.1. Standard Tensile Tests

Tensile tests are commonly performed to determine the yield strength and other characteristics of materials. Standard tensile tests are typically performed on rods of material at least 0.5 inch in diameter per ASTM A370 (ASTM, 2012). The sponsor performed standard tensile tests on the same material from the same tubes in the axial direction using the compact geometry per the standard. The data from those tests is summarized in Table 6.1. Yield strength on the raw (unstrained) metal is 112 ksi, which is within 2% of the minimum value of 110 ksi.

After strain, the metal has a slightly reduced yield strength of 95.5 ksi (average), which is a reduction of 15%. After strain aging, the metal regains some strength and is within 4% of the original value.

Table 6.1 Standard Tensile Test Data

Series	Description	YS (MPa)	UTS (MPa)	YS (ksi)	UTS (ksi)	% elongation
A370-R1	Raw	772	866	112	126	22%
A370-R2	Raw	772	868	112	126	22%
A370-E1	Strained	645	855	94	124	21%
A370-E2	Strained	669	854	97	124	20%
A370-ES1	Strained & Aged	740	881	107	128	18%
A370-ES2	Strained & Aged	765	879	111	127	19%

6.2. Raw Specimens Test Results

Table 6.2 lists the data from the mini-tensile tests performed on the raw metal alongside the results from the standard tests. There is a strong correlation, with the

mini-tensile tests yielding at 110 to 113 ksi, while the standard dogbones yielded at 112 ksi (as discussed above). The ductility of the smaller specimens was much higher at 33% compared to 22%, which is a difference of 50%. This may be due to the slower strain rate of the mini-tensile specimens versus standard specimens, which was .001 s^{-1} versus .1 s^{-1}. Dislocation movement is impeded and ductility is reduced at higher strain rates (Meier, 2012). The sponsor noted that the metal pinches the blade when the tube is first cut, indicating that residual stresses are relieved when the metal is severed. Finite element analyses have predicted the same phenomena. Therefore, smaller specimens should have less stress. These results indicate that mini-tensile tests do correlate to standard-sized test results, and may be used to draw conclusions about the relationship between axial and transverse properties.

Table 6.2 Mini-Tensile Test Results—Raw Material Only

Series	Description	L (mm)	w (mm)	t (mm)	YS (MPa)	UTS (MPa)	YS (ksi)	UTS (ksi)	% elongation
A370-R1	ASTM A370				772	866	112	126	22%
A370-R2	ASTM A370				772	868	112	126	22%
UTN	Transverse Neutral	2	1.01	0.93	774	874	112	127	33%
UTOD	Transverse OD	2	1.03	0.94	761	855	110	124	33%
UAN	Axial neutral	2	1.04	1.01	767	870	111	126	32%
UTID	Transverse ID	2	1.05	1.10	742	860	108	125	33%
UR	Radial	2	1.04	1.10	776	871	113	126	36%
	Average				764	866	111	126	33%

Comparing the transverse and axial values, the raw material had a small amount of anisotropy of approximately 0.5% (875 MPa compared to 871 MPa for the neutral axis). The data was consistent between three separate tensile tests of the same

material. The complete data set is in Appendix C. Therefore, the anisotropy of the raw metal is insignificant.

Table 6.3 contains the summary of the different sets of mini-tensile specimens, while the following figures show the stress-strain graphs. In general, the same trends seen with the standard tensile specimens are shown here: strained has a lower yield strength, while strained and aged has a higher yield strength. The strained and strained and aged stress-strain curves have sharper curves than the raw material, as shown in the graphs.

The elongation of the mini-tensile specimens cannot be compared directly to the standard tensile specimens, since the percentage is based on the length of the gage section. That is, the elongation is defined as the change in length divided by the original length. Since the original lengths of the gage sections are different (2 mm versus ~51 mm (2 inches)), the elongation percentages will be different, and they should not be directly compared. However, the elongation of the different mini-tensile specimens can be compared to each other. All of the values are 30% ± 3% (a tolerance of 10%), regardless of material. A trend is not discernable from this data.

Table 6.3 Mini-Tensile Test Results

Series	Description	L (mm)	w (mm)	t (mm)	YS (MPa)	UTS (MPa)	YS (ksi)	UTS (ksi)	% elongation
A370-R1	Raw ASTM A370[1]				772	866	112	126	22%
A370-R2	Raw ASTM A370[1]				772	868	112	126	22%
UTN	Raw Transverse, Neutral	2	1.01	0.93	774	875	112	127	33%
CTN	CNC Raw, Transverse, Neutral	2	1.04	0.91	767	821	111	119	36%
UTOD	Raw Transverse, OD	2	1.03	0.94	761	855	110	124	33%
UAN	Raw, axial, neutral	2	1.04	1.01	767	871	113	126	33%
A370-E1	Strained ASTM A370[1]				645	855	94	124	21%
A370-E2	Strained ASTM A370[1]				669	854	97	124	20%
ETN	Strained transverse neutral	2	1.01	0.97	897	929	130	135	27%
EAN	Strained axial neutral	2	0.99	0.97	793	867	115	126	31%
ESTN	Strained & aged, transverse neutral	2	1.01	0.96	933	955	135	139	26%
ESAN	Strained & aged, axial neutral	2	1.08	1.09	852	903	124	131	32%
UTID	Raw transverse ID	2	1.02	0.95	742	860	108	125	33%
UR	Raw Radial	2	1.04	1.10	776	871	113	126	36%
ER	Strained Radial	2	1.05	1.10	813	866	118	126	34%
EST	Strained & aged, Radial	2	1.04	1.09	830	898	120	130	33
EAT	Strained, Axial, Through, Average	2	1.06	1.08	792	861	115	125	32%
ETT	Strained, Transverse, Through, Average	2	1.04	1.08	817	936	119	136	32%
A370-ES1	Strained & aged ASTM A370[1]				740	881	107	128	18%
A370-ES2	Strained & aged ASTM A370[1]				765	879	111	127	19%
ESAT	Strained & aged, Axial, Through, Average	2	1.07	1.08	837	894	121	130	32%
ESTT	Strained & SA, Transverse, Through, Average	2	1.06	1.07	925	967	134	140	30%

Specimens cut sequentially from one piece of metal through the wall of the tubes (reference Figure 4.9) show a lower yield strength on the outer diameter and a slightly higher yield strength in the inner diameter. These results are summarized in Tables 6.4 (MPa) and 6.5 (ksi) and shown graphically in Figure 6.1. The stress-strain curves are

[1] Data provided by sponsor.

shown in Figures 6.2, 6.3, 6.4, 6.5, and 6.6. The strained axial (EAT) and strained transverse (ETT) specimens show a more distinct difference than the strained and strained and aged (ESAT and ESTT) specimens. This was expected, since strain-aging acts like heat treating to stress relieve the metal (Mack, 2002; see also Section 2.3).

Table 6.4 Mini-tensile Test Results—Through the Wall (MPa)

Through		EAT	ETT	ESAT	ESTT
1	OD	656	691	800	903
2		747	692	825	901
3		847	907	854	963
4		863	855	838	932
5		847	941	868	925
6	ID		861		930
	Average	792	824	837	925

Table 6.5 Mini-tensile Test Results—Through the Wall (ksi)

Location		EAT	ETT	ESAT	ESTT
1	OD	95	100	116	131
2		108	100	120	131
3		123	132	124	140
4		125	124	121	135
5		123	137	126	134
6	ID		125		135
	Average	115	120	121	134
Variance		133	204	12	9

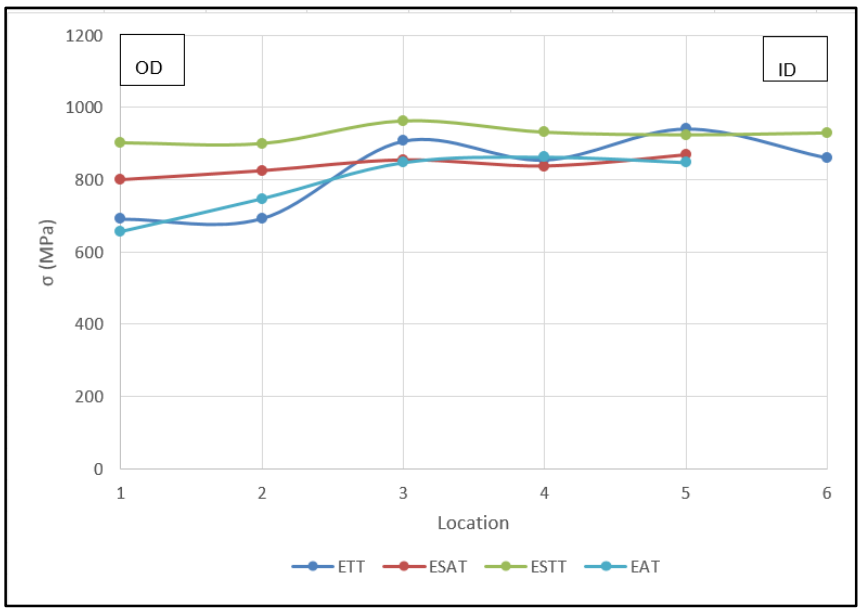

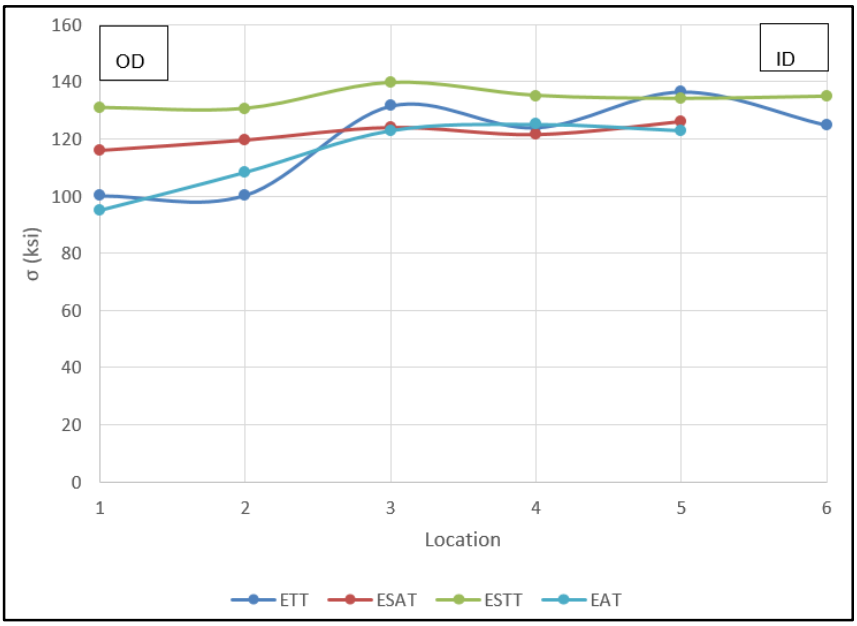

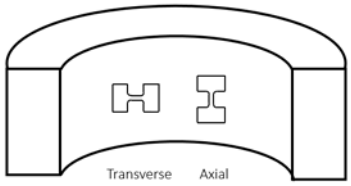

Figure 6.1 Through the Wall Graph (ETT, ESAT, ESTT, EAT) in MPa and ksi

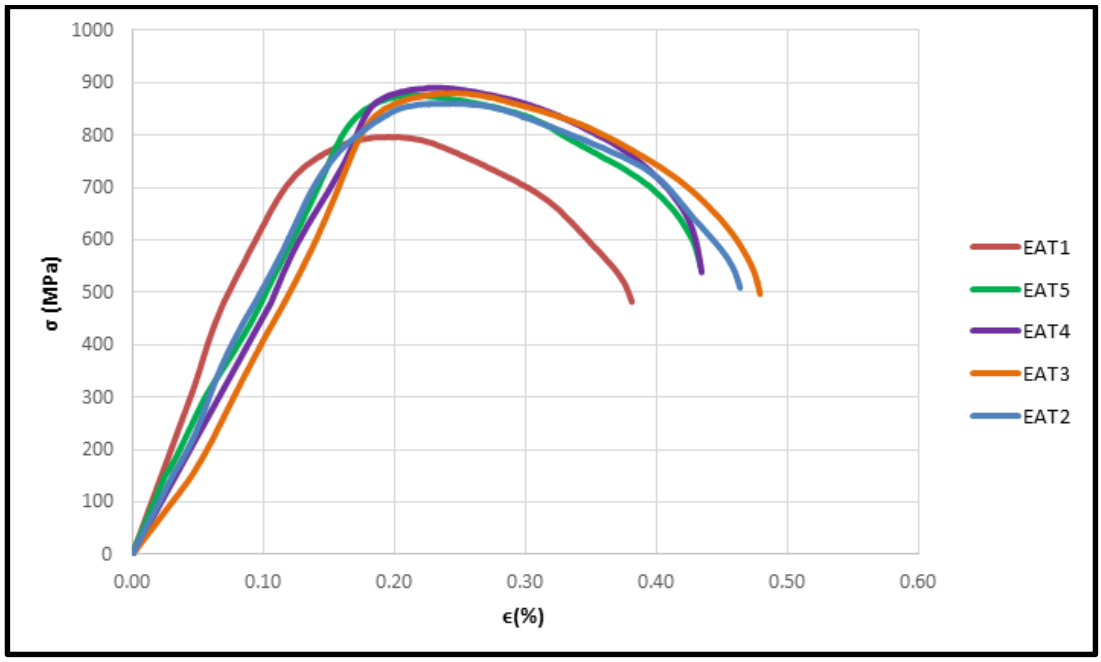

Figure 6.2 Strained Axial Through (EAT) Graph

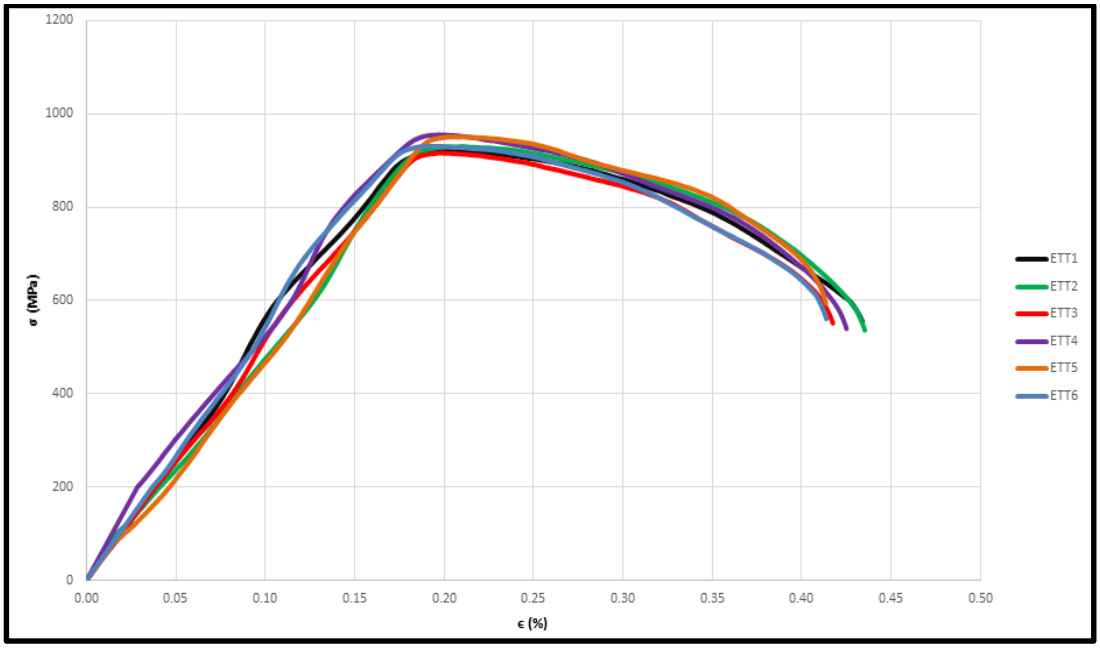

Figure 6.3 Strained Transverse Through (ETT) Graph

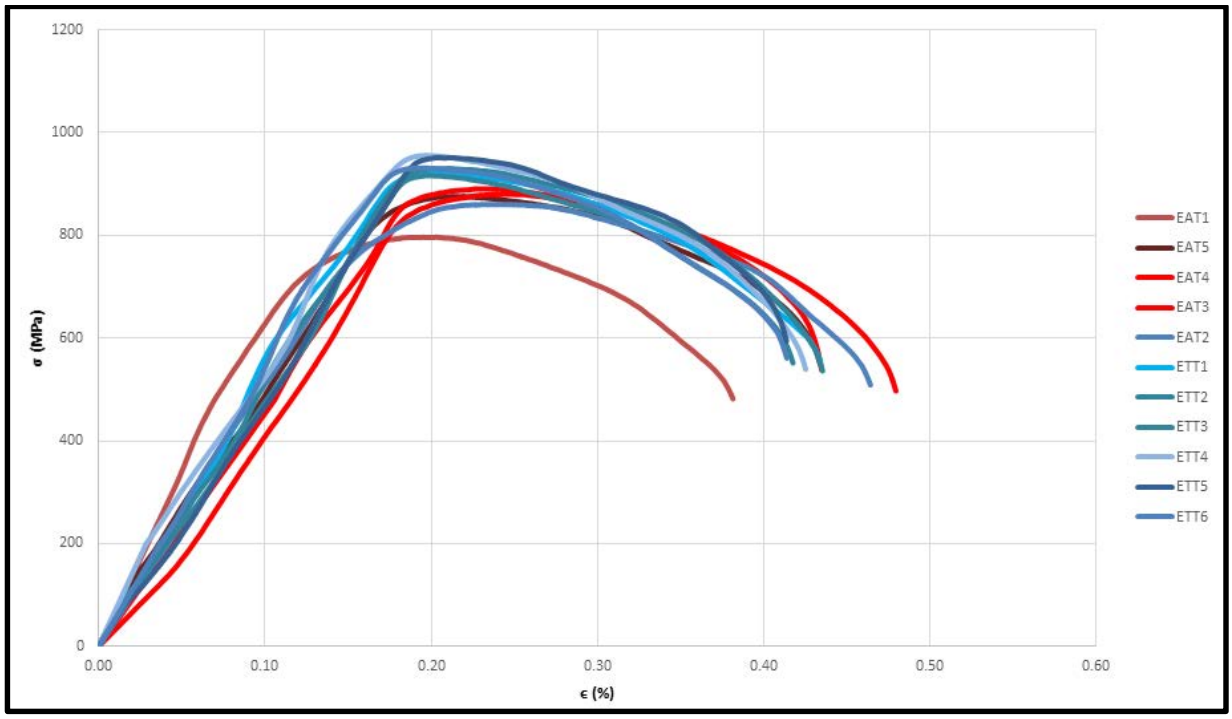

Figure 6.4 Strained Axial (EAT) and Transverse Through (ETT) Graph

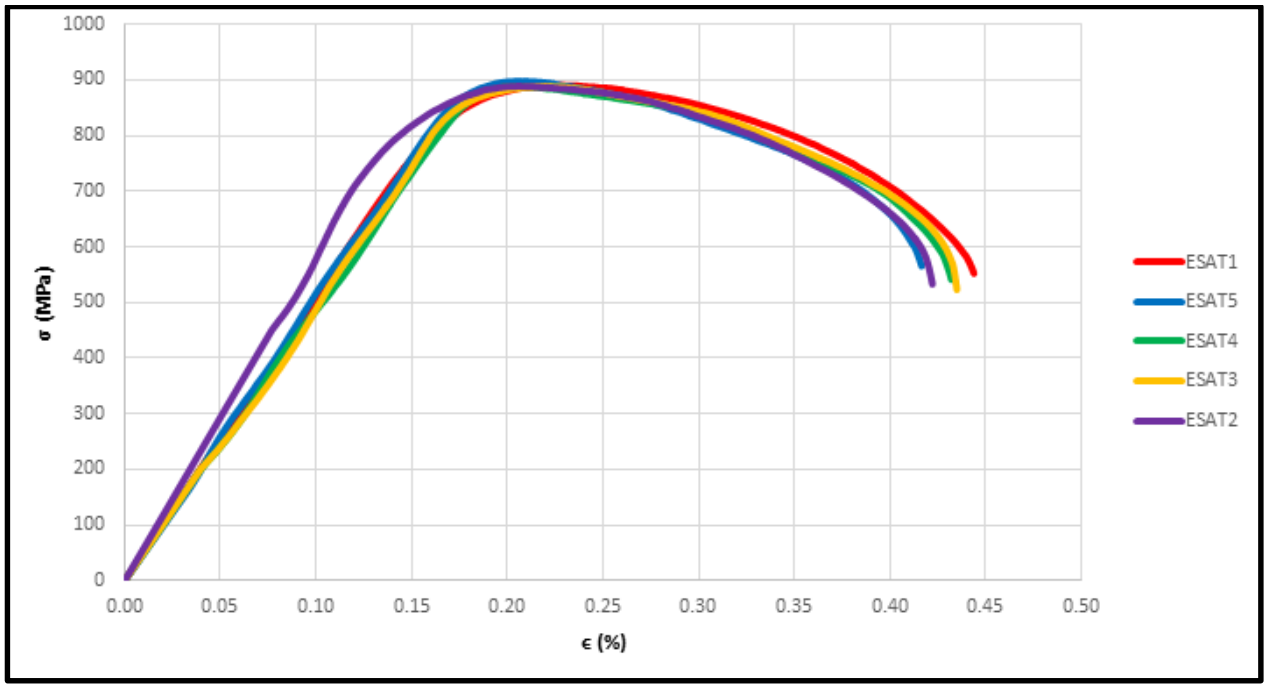

Figure 6.5 Strained and Aged Axial Through the Wall (ESAT) Graph

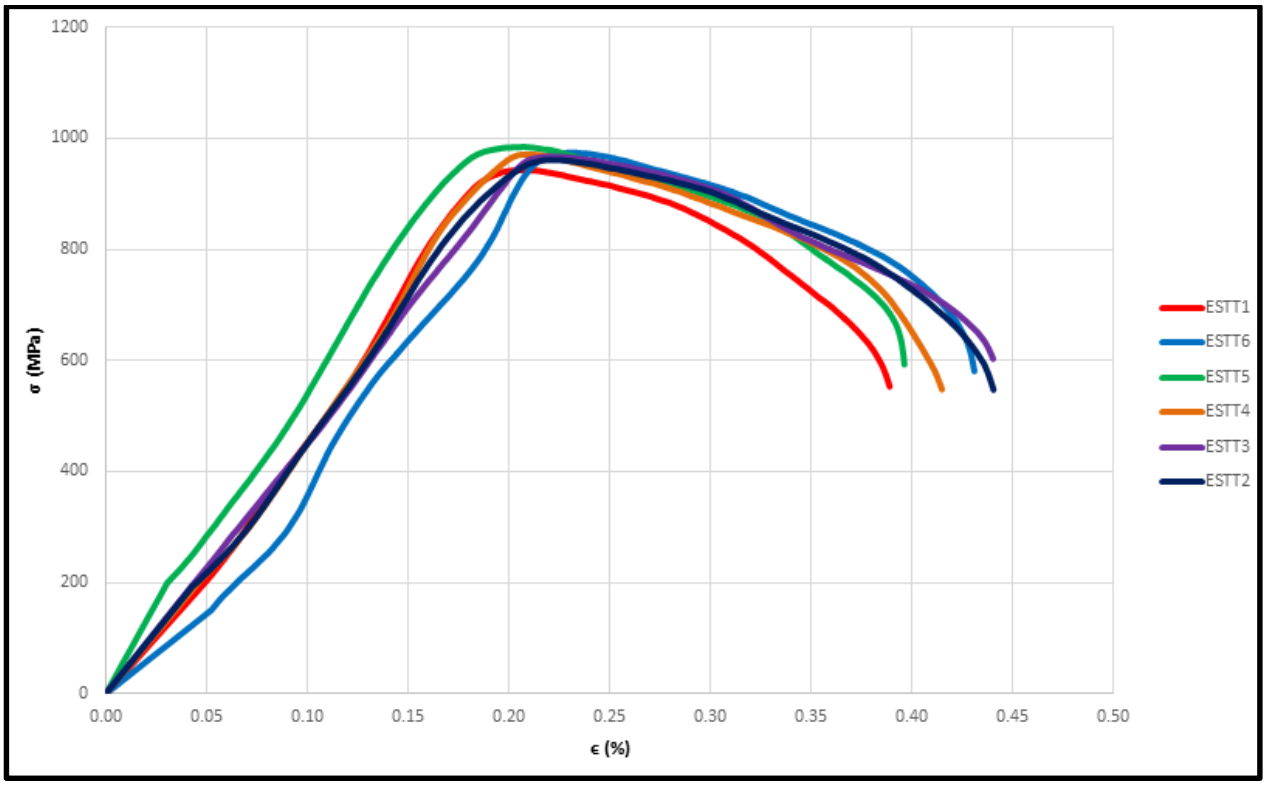

Figure 6.6 Strained and Aged Transverse Through The Wall (ESTT) Graph

Figure 6.7 shows the raw axial neutral (UAN) specimen data. This data set was redone because the sample preparation process was developed with the first set. I had experimented with 800 grit polishing pads before the 1200 grit polishing pads, which caused more damage than polishing. Therefore, the data set was re-done, and the correlation in the new set was strong. The average values are approximately the same as the UTN and CTN datasets, as expected.

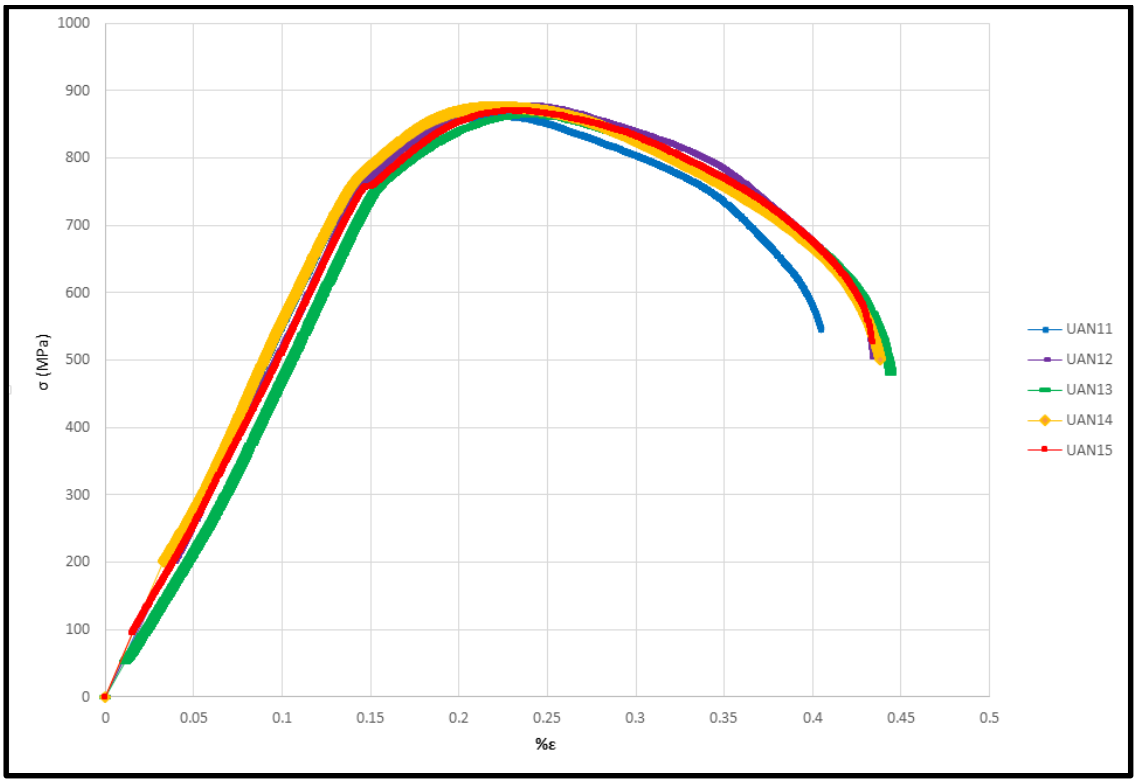

Figure 6.7 Raw Axial Neutral (UAN) Graph

The raw transverse inner diameter specimen (UTID) results are shown in Figure 6.8. These specimens were taken from the inner diameter in an attempt to measure the strain of compression from manufacturing. Figure 6.9 shows the results from the outer diameter (UTOD), which would have been tension. Figure 6.10 shows UTID and UTOD results on the same graph. The curves are very close, as are the average tensile strength values in Table 6.3. The ID yield strength is 742 MPa, while the OD is 761. If the outlier (UTID3) is ignored, then the yield strength of the ID is 753, which is within 1% of the OD yield strength. The UTS are close at 860 and 855 respectively. Therefore, the raw metal has consistent yield strength on the inner and outer diameter. This is expected, since the metal was quenched and tempered twice, per the MTR.

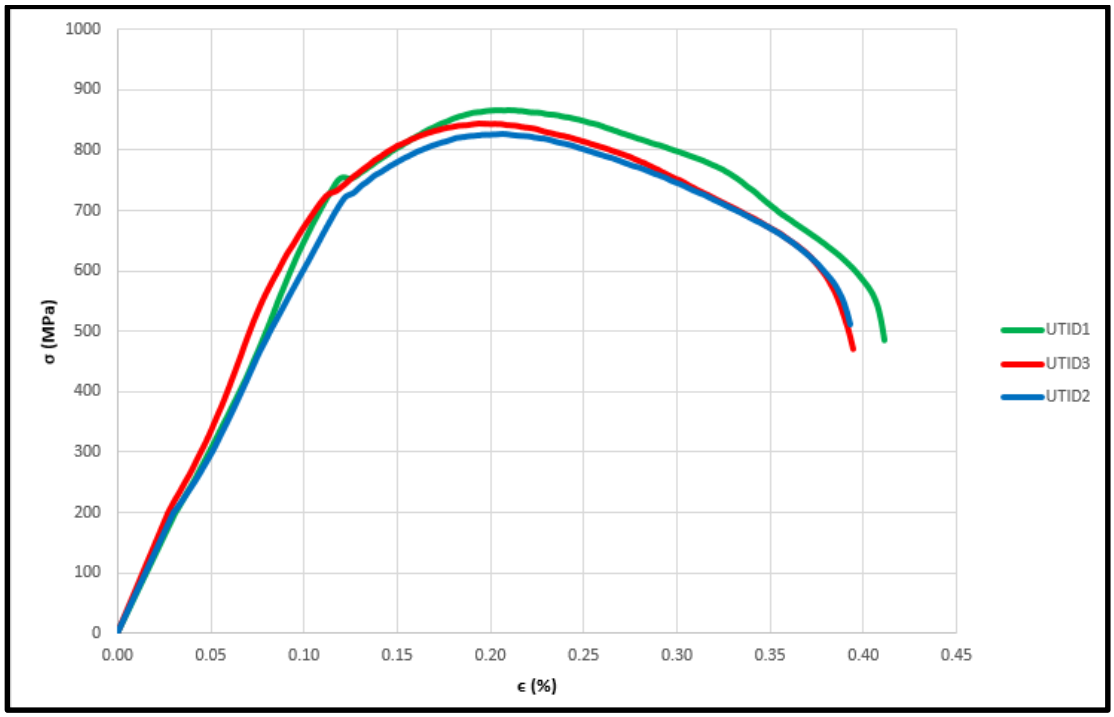

Figure 6.8 Raw Transverse Inner Diameter (UTID) Graph

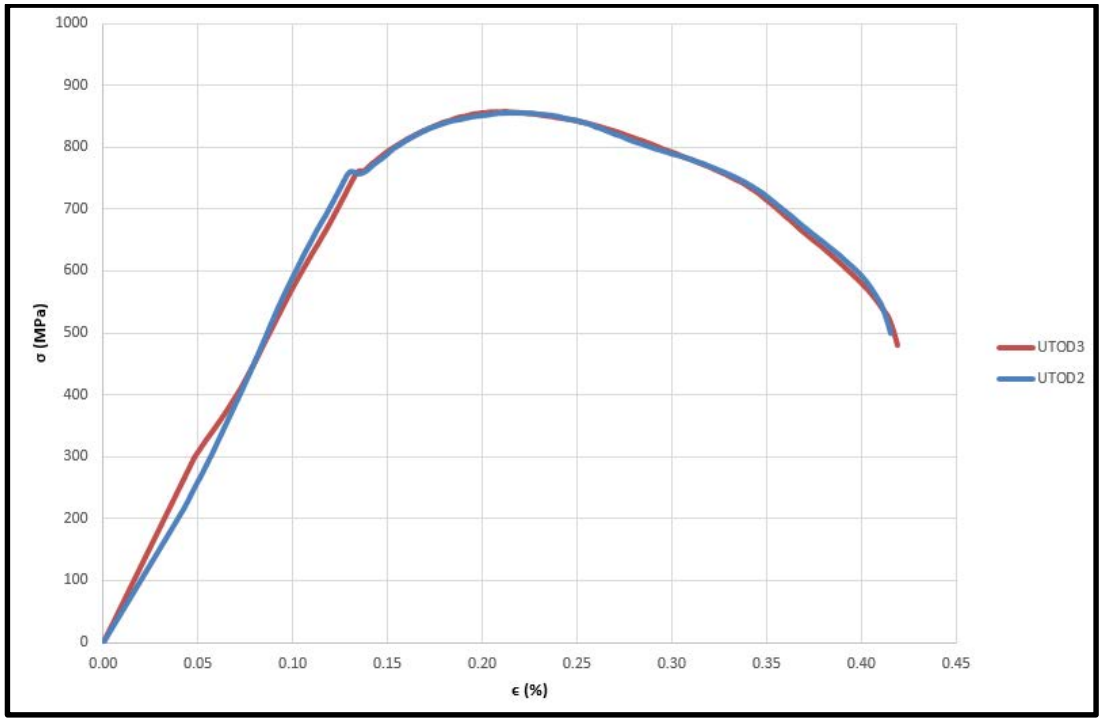

Figure 6.9 Raw Transverse Outer Diameter (UTOD) Graph

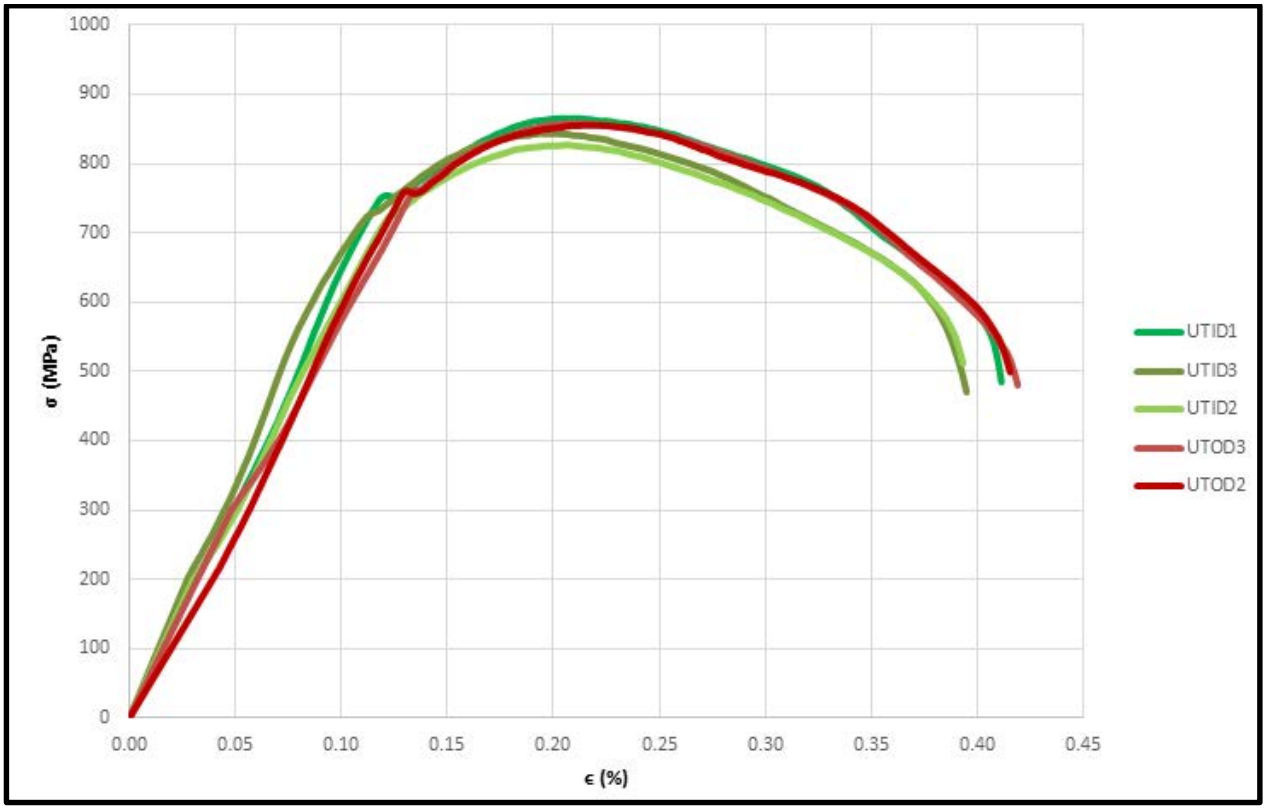

Figure 6.10 Raw Transverse Inner and Outer Diameter (UTID and UTOD) Graph

Figures 6.11 and 6.12 are the graphs of the raw and strained radial specimens, while Figure 6.13 shows both on one graph. See Figure 4.8 for clarification on the radial direction. These specimens were chosen to measure the neutral axis of the metal in addition to the transverse and axial directions, for comparison. The strained metal had an average yield strength of 813 MPa compared to 776 MPa for raw. This may indicate that the metal was work hardened at the neutral axis, which supports the findings of the Through the Wall specimens (Figure 6.1). Figure 6.14, the strained and aged radial (ESR) graph, shows a higher yield strength, which is consistent with a heat treated metal.

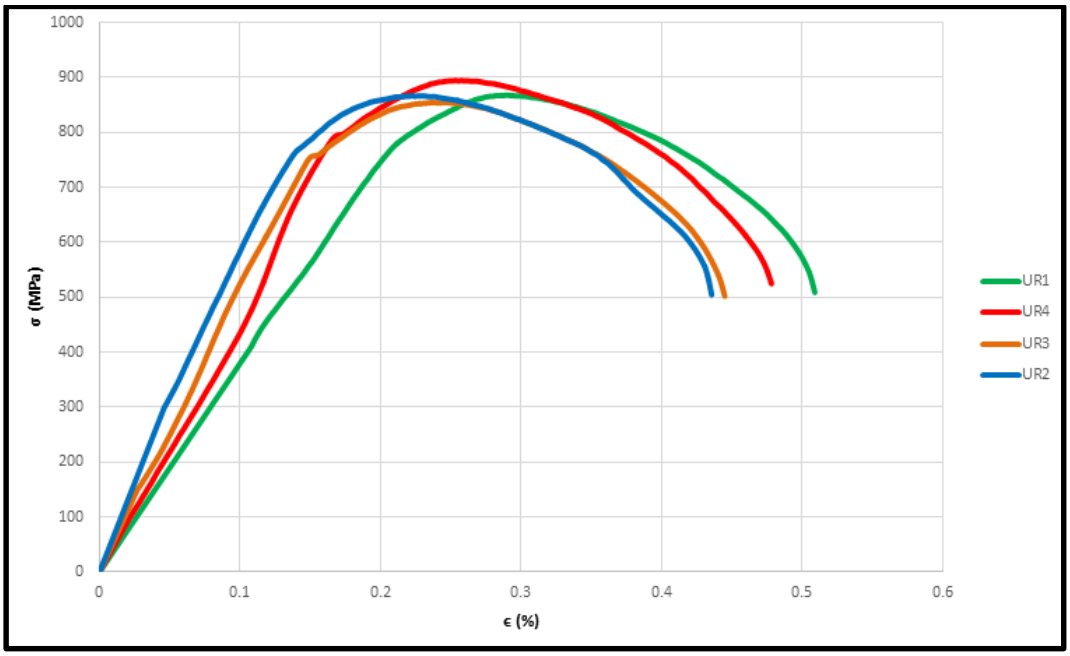

Figure 6.11 Raw Radial (UR) Graph

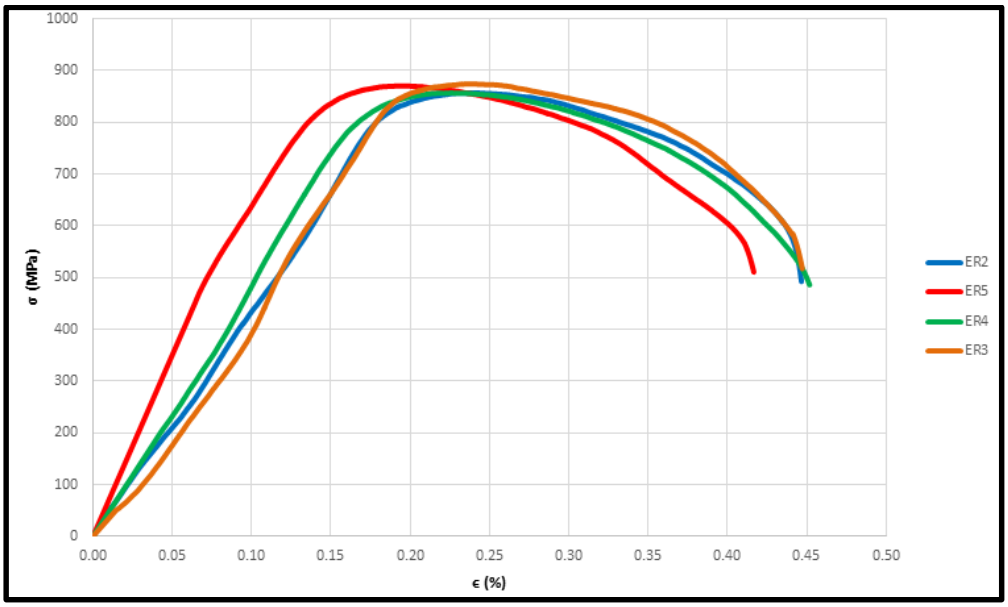

Figure 6.12 Strained Radial Graph (ER)

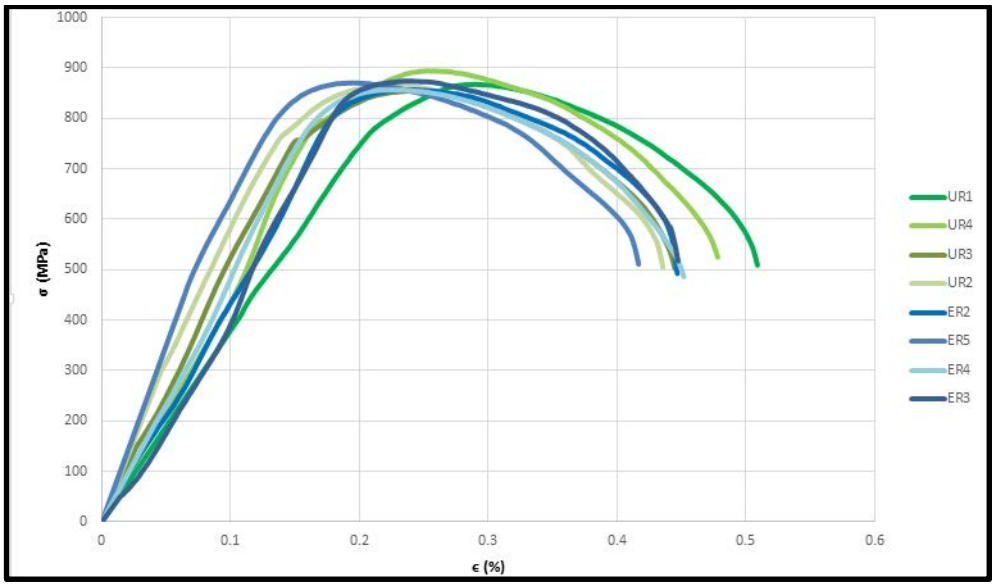

Figure 6.13 Raw and Strained Radial Graph (UR, ER) Graph

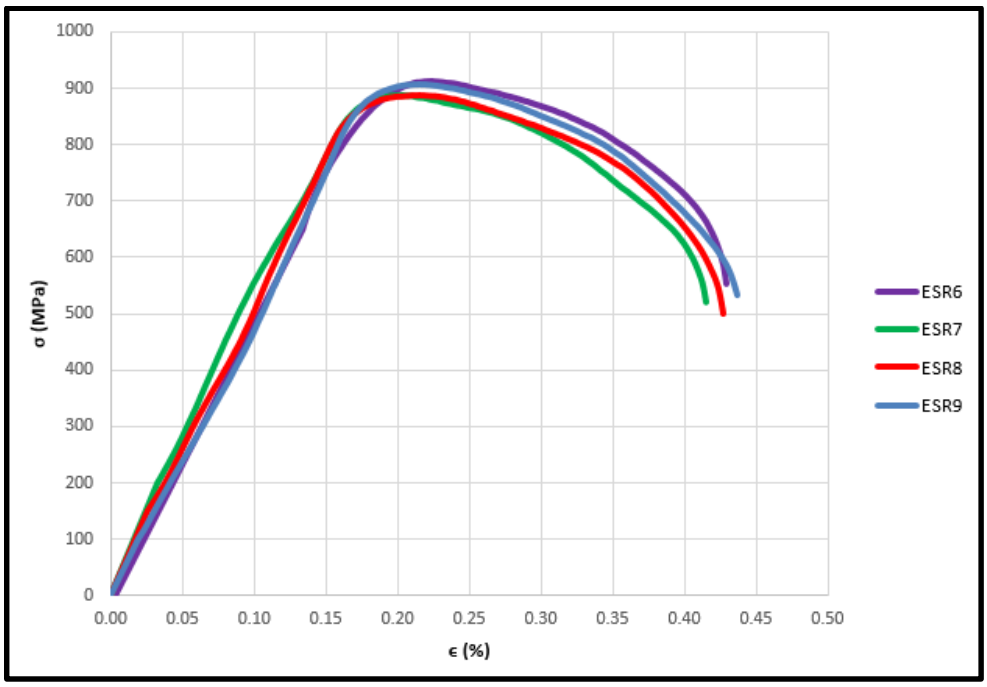

Figure 6.14 Strained and Aged Radial (ESR) Graph

Mini-tensile specimens of the strained material in the transverse (ETN) and axial (EAN) directions, along the neutral axis, are shown in Figures 6.15, 6.16, and 6.17. These may be the most important graphs to this thesis, because they show the anisotropy that was expected. Table 6.3 lists the transverse yield strength at 897 MPa and the axial yield strength at 793 MPa, a difference of 12%. See Table 6.6; the UTS is closer at 7%. Again, since strain aging is a heat treatment, lower anisotropy was expected.

The difference in the transverse (ETN) versus radial directions (ER) for strained material was slightly lower than the anisotropy in the transverse versus axial. However, the same ratio was higher for the strained and aged material (ESTN versus ESR), which was unexpected. The heat treat process should have reduced the amount of anisotropy, as it did in the transverse versus axial directions. Instead, the difference between the transverse and radial stresses increased, indicating that the radial stresses change at a slower rate than the transverse stresses. Since the radial yield stresses are lower than the transverse, they are the limiting factor. That is, those values should be used to calculate burst and collapse ratings to obtain the most conservative values.

Table 6.6 Anisotropy

Metal	Anisotropy	YS	UTS
Raw	UTN-UAN	1%	0%
Strained	ETN-EAN	12%	7%
Strained & Aged	ESTN-ESAN	9%	6%
Transverse versus Radial, Strained	ETN-ER	9%	7%
Transverse versus Radial, Strained & Aged	ESTN-ESR	11%	6%

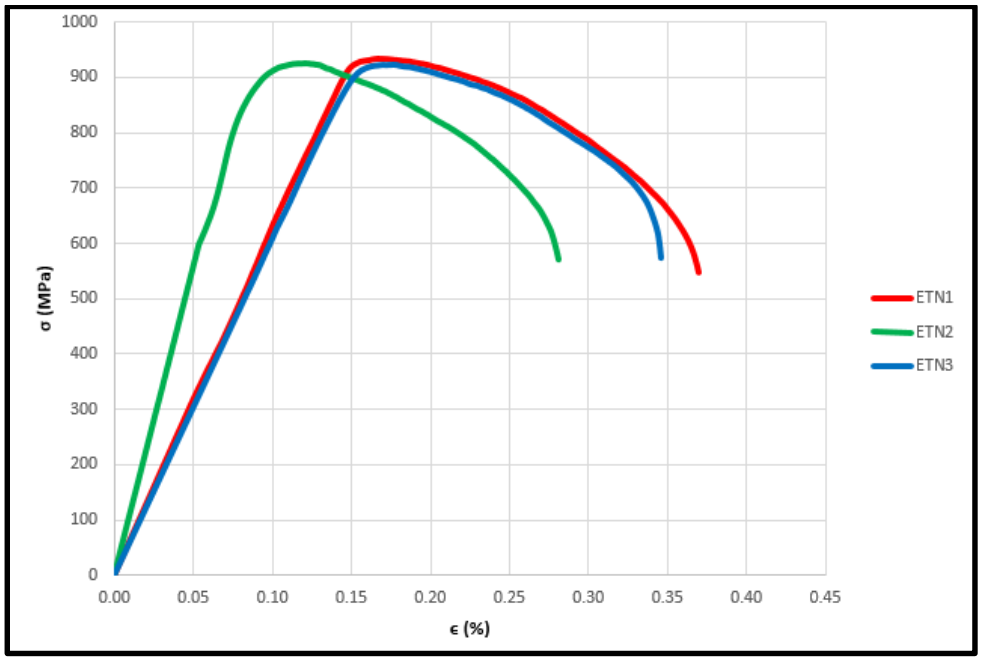

Figure 6.15 Strained Transverse Neutral (ETN) Graph

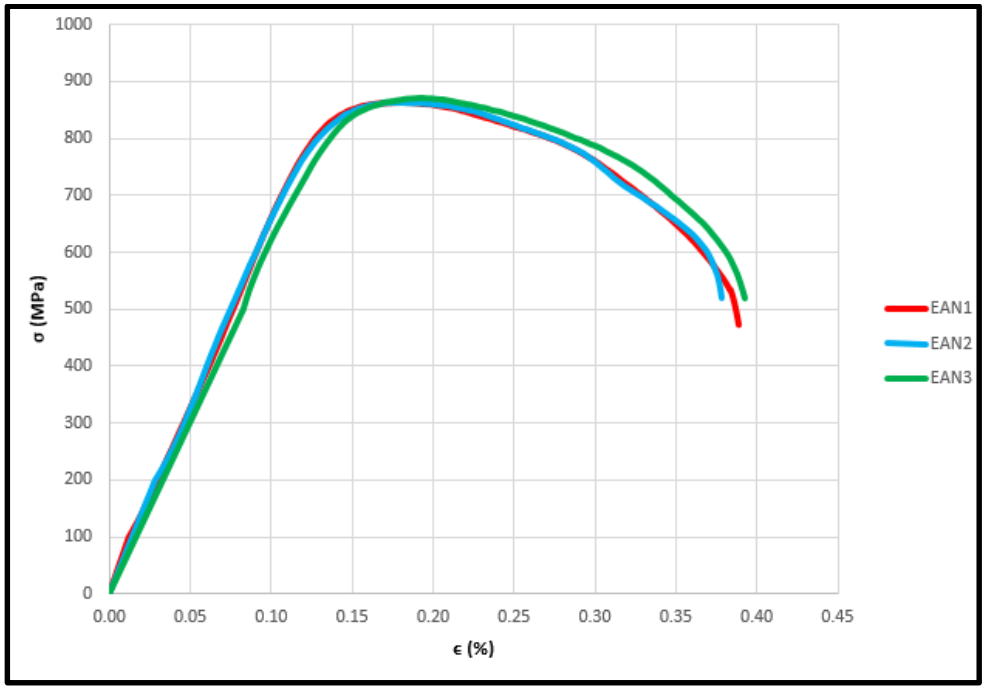

Figure 6.16 Strained Axial Neutral (EAN) Graph

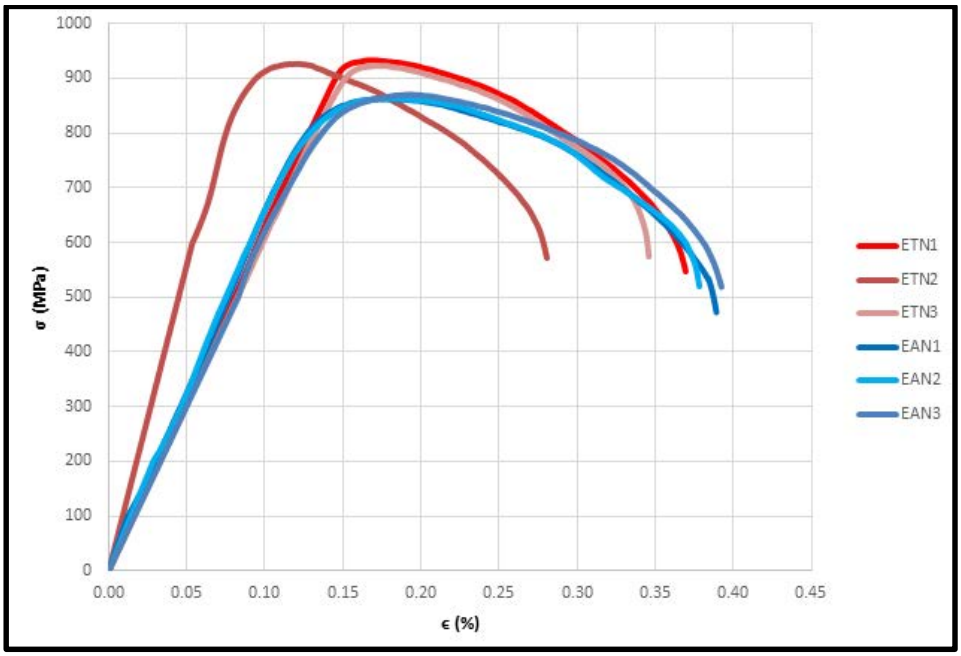

Figure 6.17 Strained Transverse Neutral (ETN) and Strained Axial Neutral (EAN) Graph

The strained and aged data sets (ESTN and ESAN) have less anisotropy, as shown in Figures 6.18, 6.19, and 6.20, and Table 6.6. These lowered values are the result of the stress relaxation of the strain aging process, which is a heat treatment (Mack, 2002).

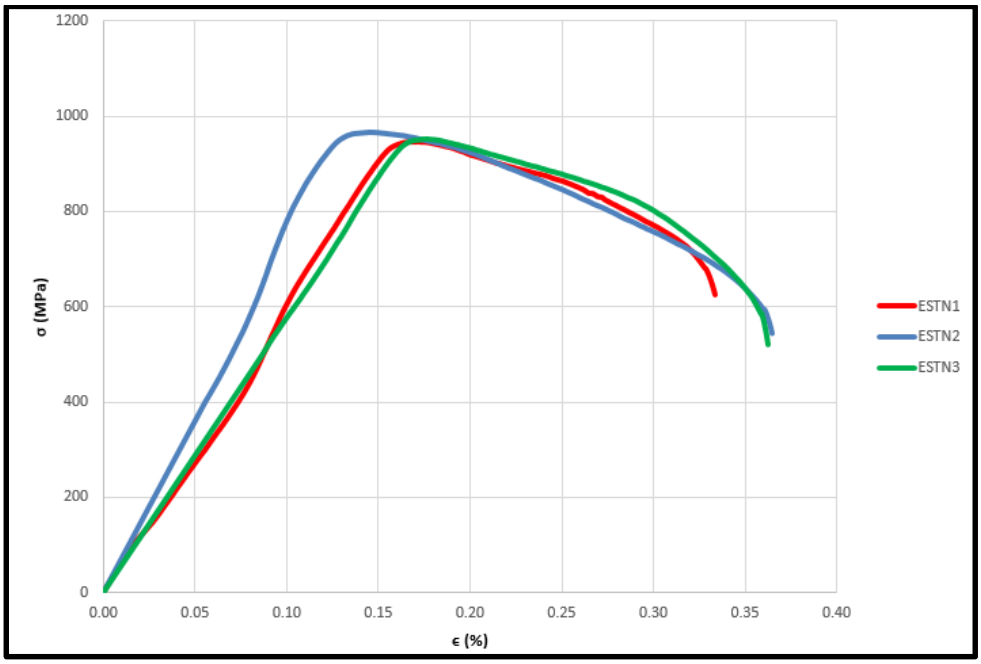

Figure 6.18 Strained and Aged Transverse Neutral (ESTN) Graph

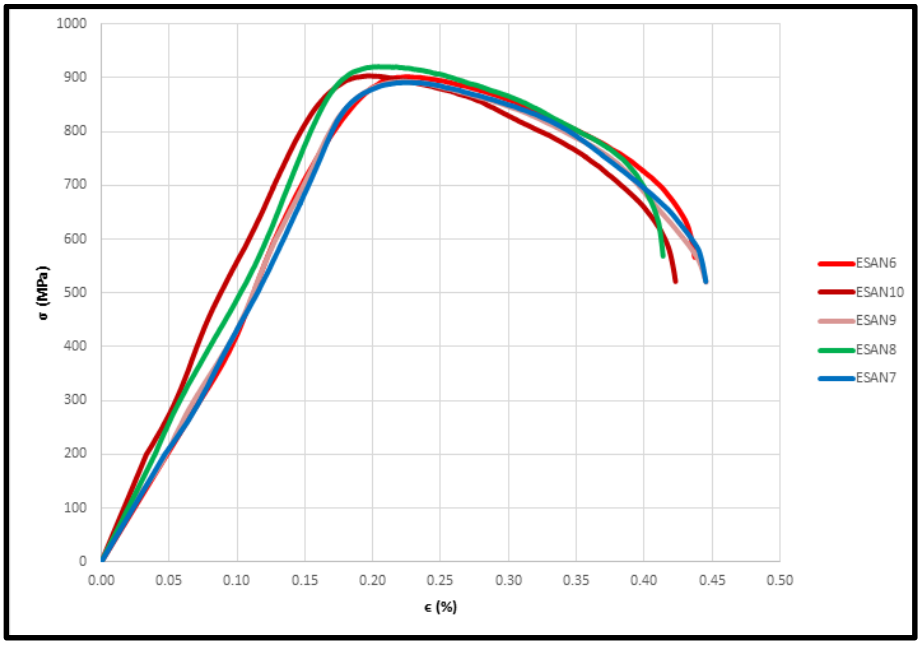

Figure 6.19 Strained and Aged Axial Neutral (ESAN) Graph

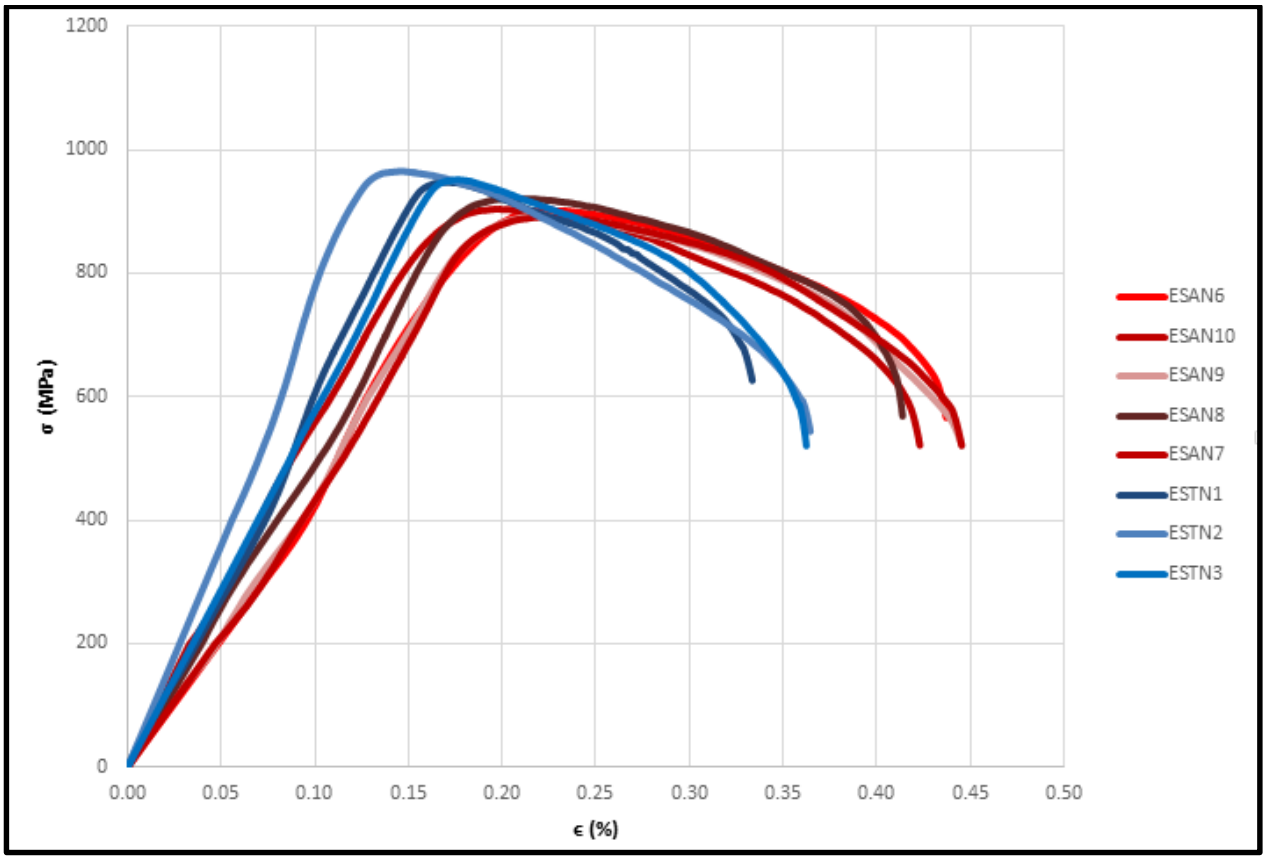

Figure 6.20 Strained and Aged Transverse (ESTN) and Axial Neutral (ESAN) Graph

Figure 6.21 shows the axial values on one graph for comparison, while Figure 6.22 shows the transverse.

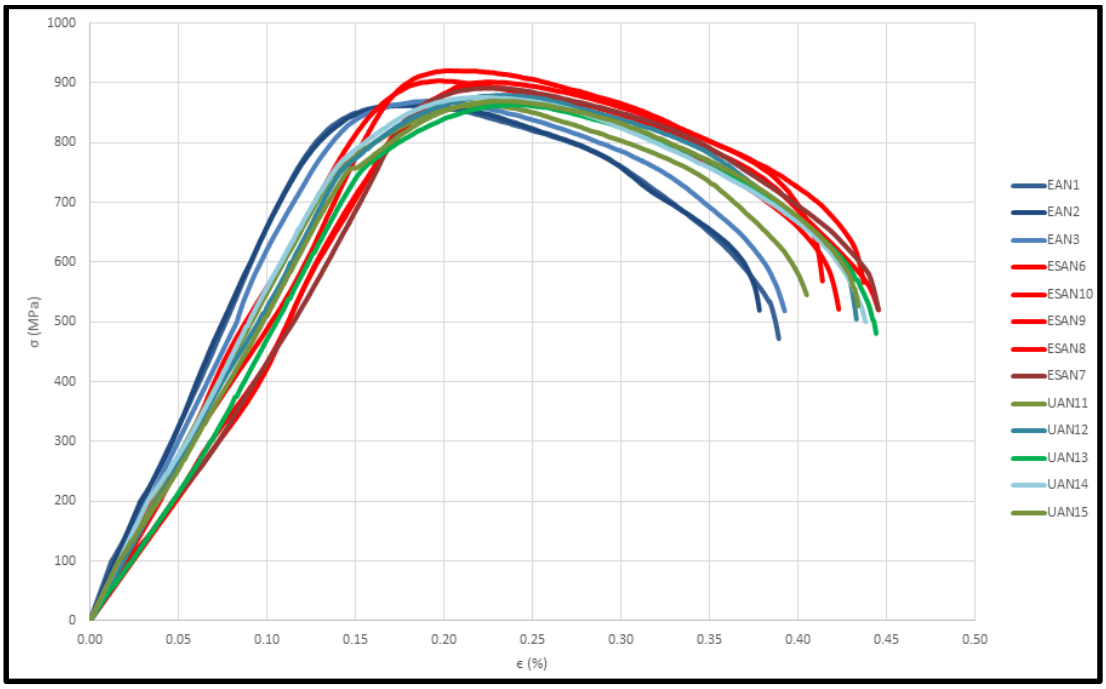

Figure 6.21 Axial: Raw, Strained, Strained and Aged (UAN, EAN, ESAN) Graph

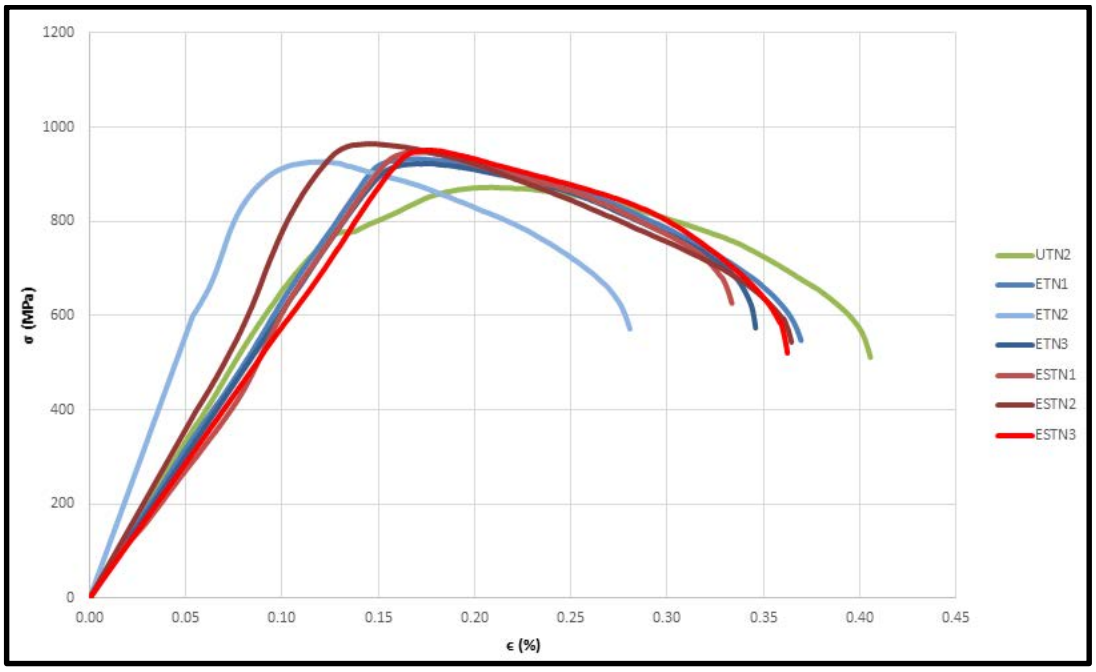

Figure 6.22 Transverse: Raw, Strained, Strained and Aged (UTN, ETN, ESTN) Graph

7. CONCLUSION

I set out to characterize the anisotropic nature of swaged metal. As expected, the tensile tests showed a difference between the axial and transverse tensile strength. The correlation was 12% difference in yield strength in the axial and transverse directions for strained material and 9% in strained and aged material. This means that the strength of the metal in the hoop (transverse) direction is approximately 10% stronger than in the axial direction, because the metal was work hardened during the swaging process. Therefore, the metal is more likely to fail in axial tension than in burst or collapse.

I presented the findings from the microstructure examination, standard tensile tests, and SEM data. All of this data supported the findings of the mini-tensile tests. This information will help engineers set burst and collapse ratings and allow material scientists to predict the anisotropic characteristics of swaged steel tubes.

8. RECOMMENDATIONS

Since the strained metal has a higher yield strength than the raw material, using the raw yield strength to calculate burst and collapse ratings is a conservative method. The metal has even higher yield strength after strain aging, which indicates that the stresses in the metal are relieved during the process. Even with the 12% anisotropy in the strained and 9% anisotropy in the strain aged specimens, the raw yield strengths are lower and therefore more conservative. I recommend that the sponsor continue using the raw yield strength to calculate these ratings.

Though this thesis is complete and I have confidence in the results, further research could be performed as follows:

1. Test another heat of the same mild steel to confirm the conclusions.
2. Repeat the mini-tensile tests on another steel alloy to see if similar results are obtained.
3. Perform tests with longer gage specimens per ASTM for comparison (reference Section 2.3).
4. Find a reliable way to electropolish and/or chemical polish the steel and repeat the mini-tensile tests to determine whether surface effects were a factor.
5. Perform the tests with different strain rates. Use .1 s-1 for a more direct comparison to the standard tensile tests (reference Section 6.2).
6. Perform nanohardness tests and capture more SEM images to study the banding.

7. Investigate the banding effect of manganese and the role that it plays in fracture.
8. Perform mini-tensile test in the SEM to determine whether the bands play a role.
9. Perform further research on the recast layer.

9. APPENDICES

These appendices contain supplemental information. While this information may be too detailed for some readers, others may find it useful.

9.1. Appendix A – Mini-Tensile Test Procedure

The steps for the tests were as follows:

1. Polish the specimen and dip in methanol. Keep specimen with the bag labeled with the series and specimen number (ex. UTOD1).
2. Measure the specimen's width (w) and thickness (t) using calipers.
3. Enter w and t into the GUI. Press "stop" then "run" at the top of the toolbar to save the data.
4. Create a new text file into which the data will be recorded (ex. 12_04_05_UTOD1.txt)
5. Place the specimen in the grips on the machine. Move the grips toward each other using the manual cross-head movement button (Figure 4.15 where the cursor is pointing). The movement value should be negative.
6. Preload the machine by pushing the manual cross-head movement button. The movement value should be positive. Watch the load value on the display (Figure 4.11, upper right hand corner) and stop at -3.00 lbs. Note that the unloaded value on the display is typically -6.66.
7. Initialize the data acquisition software.
8. Double check all values and the name of the text file.
9. Start the test by pressing "Start Test."
10. The test will run for approximately 15-20 minutes.

11. When the sample breaks, the curve on the screen will drop off (as shown in Figure 4.12) and a “pop” will be heard. Press “DAQ Stop.”

9.2. Appendix B – Data Analysis

The data collected during the test includes time (seconds), displacement (mm), load (newtons), strain (mm/mm), and stress (MPa). This raw data is analyzed using OriginPro 8.5.1 SR2 software. The steps include:

1. Create “Time Zeroed” column equal to time minus the initial time (T_0). Ex. If the first time listed is 5.21 seconds and Col(A) is time, then the Time Zeroed column would be:

$$Time\ Zeroed = Col(A) - T_0 = Col(A) - 5.21$$

2. Create “Fixed Stress” column equal to stress minus the value on the digital screen at zero divided by the cross-section of the specimen. That is, the load does not have tare function, so the calculation must be done manually. Ex. If the screen displays -6.67 pounds (a typical value), then the conversion factor of 4.45 newtons/pound must be used. The thickness of the specimen is 1.00 mm and the width is 1.00 mm. The equation becomes

$$Fixed\ Stress = Col(E) - \frac{Preload * 4.45}{w * t} = Col(E) - \frac{-6.67 * 4.45}{1.00 * 1.00} = Col(E) + 29.68$$

Since the cross-sections of all of the specimens and the initial value were roughly the same, the value 29.68 was used to analyze all the data.

3. Create “Fixed Strain” column equal to displacement (x) minus initial displacement (x_0) divided by the gage length.

$$Fixed\ Strain = \frac{x - x_0}{2} = \frac{Col(B) - x_0}{2}$$

4. Create a graph of Fixed Stress versus Time Zeroed.
5. Smooth the function using the Savitzky-Golay method with 50 points of window (explained in section 4.4 below). This creates a new function on the same graph which is called Smoothed Stress.
6. Create a graph of Fixed Strain versus Time Zeroed.
7. Smooth the function using the FFT filter and 150 points (explained in section 4.4 below). This creates a new function on the same graph which is called Smoothed Strain.
8. Create a graph of Smoothed Stress versus Smooth Strain.
9. Draw line in elastic region (where the function is relatively straight) over the function.
10. Copy and paste the line. This creates an identical line with the same slope. Move it 0.02% to the right of the existing function. Note that if the function hits the origin, then the x-axis value will be 0.0002. However, if the function crosses the x-axis at another value, then add that value to 0.0002. Example if the function crosses the x-axis at 0.001, then the new line should cross the x-axis at 0.0012.
11. Record the value where the new line hits the function. This is the 0.02% Offset Yield Stress.
12. Record the maxima of the function. This is the ultimate tensile strength (UTS).

13. Copy and paste the line again. Move it to where it hits the end of the curve.
14. Record the difference between the function's x-axis value and newest line's x-axis value. This is the elongation.

The values are entered into a table in Excel. The series are averaged for the summary tables. Graphs were made from the smoothed data.

Smoothing Functions

The data analysis included use of the FFT filter and Savitzky-Golay signal processing. FFT filtering uses Fourier transforms, while Savitzky-Golay uses polynomial expansion. These are complex mathematical concepts that are outside the scope of this paper.

9.3. Appendix C – Mini-Tensile Test Data

The Young's Modulus values are listed in the table below are skewed due to the compliance of the mini-tensile test machine. Elastometers (either mini or laser) would be required to generate a true stress-strain curve, which would have a valid Young's Modulus.

Sample	Description	L (mm)	w (mm)	t (mm)	YS (MPa)	UTS (MPa)	% el	Young's Modulus
UTN1	Raw, EDM, Transverse, Neutral	2	1.01	0.94	775	875	33%	NA
UTN2	Raw, EDM, Transverse, Neutral	2	1.01	0.92	772	873	34%	6628
UTN	**Average**	**2**	**1.01**	**0.93**	**774**	**874**	**33%**	**6628**
CTN1	CNC Raw, Transverse, Neutral	2	1.08	0.91	782	881	35%	6173
CTN3	CNC Raw, Transverse, Neutral	2	1.03	0.91	752	760	37%	6181
CTN	**Average**	**2**	**1.06**	**0.91**	**767**	**821**	**36%**	**6177**
UTOD1	Raw, EDM, Transverse, OD	2	1.03	0.94	750	851	34%	NA
UTOD2	Raw, EDM, Transverse, OD	2	1.03	0.94	761	856	33%	5920
UTOD3	Raw, EDM, Transverse, OD	2	1.03	0.94	772	859	34%	5702
UTOD	**Average**	**2**	**1.03**	**0.94**	**761**	**855**	**33%**	**5811**
UAN11	Raw, axial, neutral	2	1.00	1.05	763	863	31%	5477
UAN12	Raw, axial, neutral	2	1.08	1.00	769	881	34%	5283
UAN13	Raw, axial, neutral	2	1.07	1.01	767	865	34%	4822
UAN14	Raw, axial, neutral	2	1.08	1.00	779	876	35%	5558
UAN15	Raw, axial, neutral	2	1.08	1.00	760	872	33%	5100
UAN	**Average**	**2**	**1.05**	**1.06**	**766**	**865**	**32%**	**5248**
ETN1	Strained transverse neutral	2	1.01	0.96	904	935	28%	6243
ETN2	Strained transverse neutral	2	1.01	0.96	883	928	26%	6108
ETN3	Strained transverse neutral	2	1	0.98	905	924	25%	6075
ETN	**Average**	**2**	**1.01**	**0.97**	**897**	**929**	**27%**	**6142**
EAN1	Strained axial neutral	2	0.99	0.98	812	864	32%	6529
EAN2	Strained axial neutral	2	1	0.97	773	865	30%	6614
EAN3	Strained axial neutral	2	0.99	0.97	793	872	31%	5007
EAN	**Average**	**2**	**0.99**	**0.97**	**793**	**867**	**31%**	**6050**
ESTN1	Strained & aged, transverse neutral	2	1.02	0.97	934	950	23%	6091
ESTN2	Strained & aged, transverse neutral	2	1	0.96	926	965	30%	7443
ESTN3	Strained & aged, transverse neutral	2	1.02	0.96	939	952	27%	5754
ESTN	**Average**	**2**	**1.01**	**0.96**	**933**	**955**	**26%**	**6429**
ESAN6	Strained & aged, axial neutral	2	1.07	1.15	814	900	32%	5064

ESAN7	Strained & aged, axial neutral	2	1.08	1.08	856	893	33%	5061
ESAN8	Strained & aged, axial neutral	2	1.08	1.06	888	923	30%	5029
ESAN9	Strained & aged, axial neutral	2	1.08	1.09	847	893	33%	4322
ESAN10	Strained & aged, axial neutral	2	1.08	1.08	853	904	33%	5625
ESAN	**Average**	**2**	**1.08**	**1.09**	**852**	**903**	**32%**	**5020**
UTID1	Raw transverse ID	2	1.01	0.94	752	867	34%	6133
UTID2	Raw transverse ID	2	1.04	0.96	753	866	34%	6040
UTID3	Raw transverse ID	2	1.02	0.95	720	846	33%	6830
UTID	**Average**	**2**	**1.02**	**0.95**	**742**	**860**	**33%**	**6334**
ER2	Strained Radial	2	1.05	1.10	833	858	33%	4292
ER2	Strained Radial	2	1.05	1.09	844	875	33%	3204
ER4	Strained Radial	2	1.06	1.10	772	858	35%	4646
ER5	Strained Radial	2	1.05	1.09	802	872	34%	4692
ER	**Average**	**2**	**1.05**	**1.10**	**813**	**866**	**34%**	**4209**
ESAT1	Strained & Aged, Axial, Through	2	1.05	1.06	800	891	33%	5307
ESAT2	Strained & Aged, Axial, Through	2	1.07	1.09	825	890	33%	6753
ESAT3	Strained & Aged, Axial, Through	2	1.08	1.09	854	900	33%	5247
ESAT4	Strained & Aged, Axial, Through	2	1.08	1.09	838	890	32%	4845
ESAT5	Strained & Aged, Axial, Through	2	1.08	1.09	868	898	30%	5046
ESAT	**Average**	**2**	**1.07**	**1.08**	**837**	**894**	**32%**	**5440**
UR1	Raw Radial	2	1.05	1.10	788	867	37%	3593
UR2	Raw Radial	2	1.05	1.10	767	868	35%	3612
UR3	Raw Radial	2	1.05	1.11	752	854	35%	5160
UR4	Raw Radial	2	1.02	1.08	796	895	37%	6049
UR	**Average**	**2**	**1.04**	**1.10**	**776**	**871**	**36%**	**4604**
ESR6	E&SA, Radial	2	1.03	1.08	786	912	31%	5266
ESR7	E&SA, Radial	2	1.03	1.10	843	890	32%	5631
ESR8	E&SA, Radial	2	1.05	1.09	844	888	33%	5114
ESR9	E&SA, Radial	2	1.03	1.09	858	909	36%	4671
ESR	**Average**	**2**	**1.04**	**1.09**	**830**	**898**	**33%**	**5517**
EAT1	Strained, Axial, Through	2	1.02	1.05	656	796	26%	4969
EAT2	Strained, Axial, Through	2	1.08	1.10	747	860	36%	5094
EAT3	Strained, Axial, Through	2	1.08	1.08	847	879	36%	5020
EAT4	Strained, Axial, Through	2	1.06	1.09	863	891	31%	4668
EAT5	Strained, Axial, Through	2	1.07	1.10	847	877	32%	4906
EAT	**Average**	**2**	**1.06**	**1.08**	**792**	**861**	**32%**	**4931**
ETT1	Strained, Transverse Through	2	1.04	1.04	691	922	33%	5126
ETT2	Strained, Transverse Through	2	1.05	1.09	692	932	33%	4955
ETT3	Strained, Transverse Through	2	1.06	1.10	907	918	31%	5057
ETT4	Strained, Transverse Through	2	1.04	1.08	855	956	34%	4730
ETT5	Strained, Transverse Through	2	1.03	1.08	941	953	29%	5389
ETT6	Strained, Transverse Through	2	1.04	1.09	861	932	31%	5341

ETT	**Average**	**2**	**1.04**	**1.08**	**817**	**936**	**32%**	**5051**
ESTT1	E&S, Transverse Through	2	1.05	1.00	903	946	27%	5779
ESTT2	E&S, Transverse Through	2	1.06	1.09	901	960	32%	5324
ESTT3	E&S, Transverse Through	2	1.06	1.08	963	968	31%	4525
ESTT4	E&S, Transverse Through	2	1.05	1.10	932	970	31%	4730
ESTT5	E&S, Transverse Through	2	1.05	1.07	925	987	29%	5245
ESTT6	E&S, Transverse Through	2	1.06	1.07	930	974	29%	5332
ESTT	**Average**	**2**	**1.06**	**1.07**	**925**	**967**	**30%**	**5156**

9.4. Appendix D – Graph Shifts

The compliance of the machine causes small curves at the beginning of the stress-strain curves. That is, the mini-tensile machine absorbs some of the stress, which is shown on the graph as a small curve (Figure D.1). The linear region should cross the x-axis at the origin. Steps taken to correct the graphs include:

1. Graph stress-strain curve (see Section 9.2, Appendix B).
2. Determine the linear region (ex. stress ranges from 200 to 900 MPa, highlighted in Figure D.1)
3. Graph the linear region on a separate graph (Figure D.3).
4. Insert the equation of the line using the Trendline function in Excel. The line equation is in the form y=mx+b, which for this graph is $\sigma = E\varepsilon + b$. The graph is shifted to the right by b; that is, b should be zero.
5. Rename strain column from “e_ETN1” to “e_ETN1_old” to indicate that is the original data.
6. Create new column named “e_ETN1.” Populate with the equation =e_ETN1_old – b.
7. Insert Point (0,0) by adding a row with e_ETN1 equal to zero and ETN1 (stress) equal to zero.

8. Delete rows up to where the graph becomes linear.

9. Graph e_ETN1 (strain) versus ETN1 (stress)

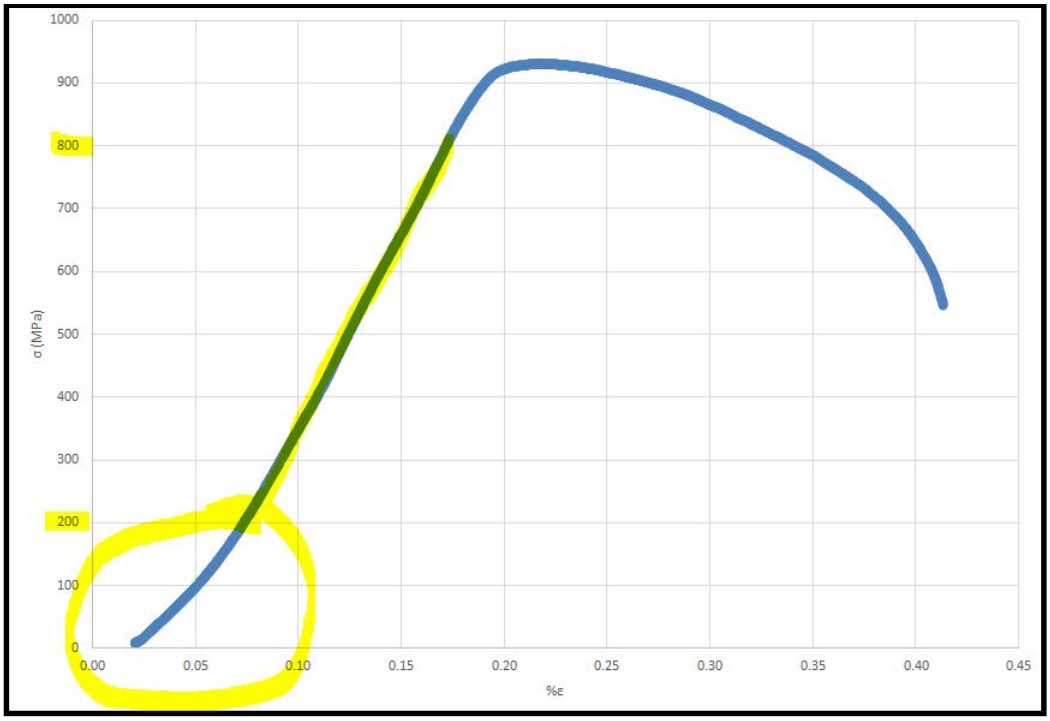

Figure D.1 Specimen ETN1 Stress-Strain Curve (Uncorrected)

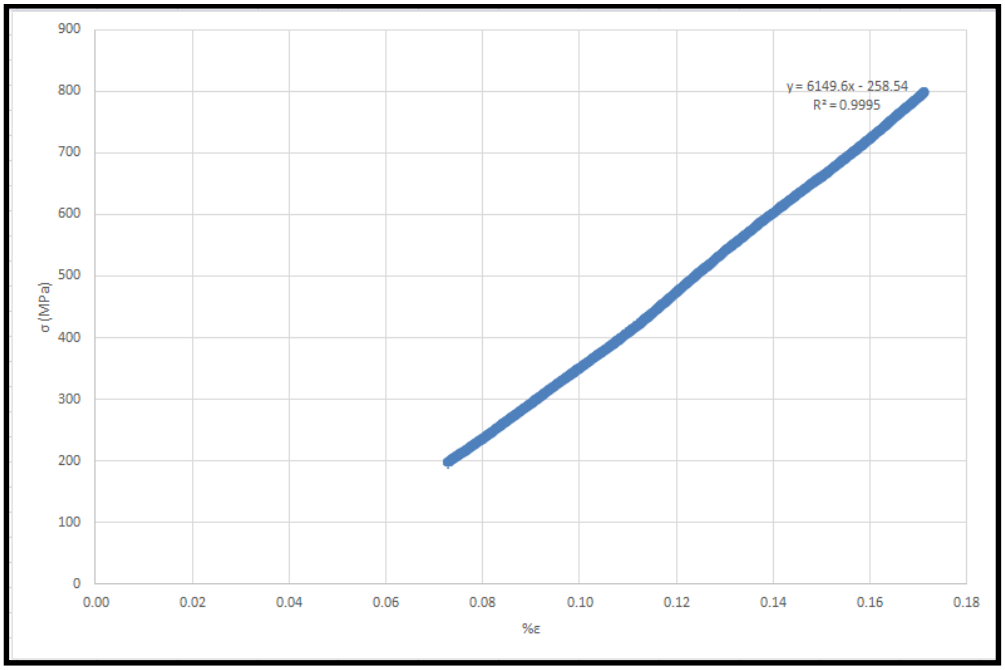

Figure D.2 Graph of the Linear Region with Trend Line

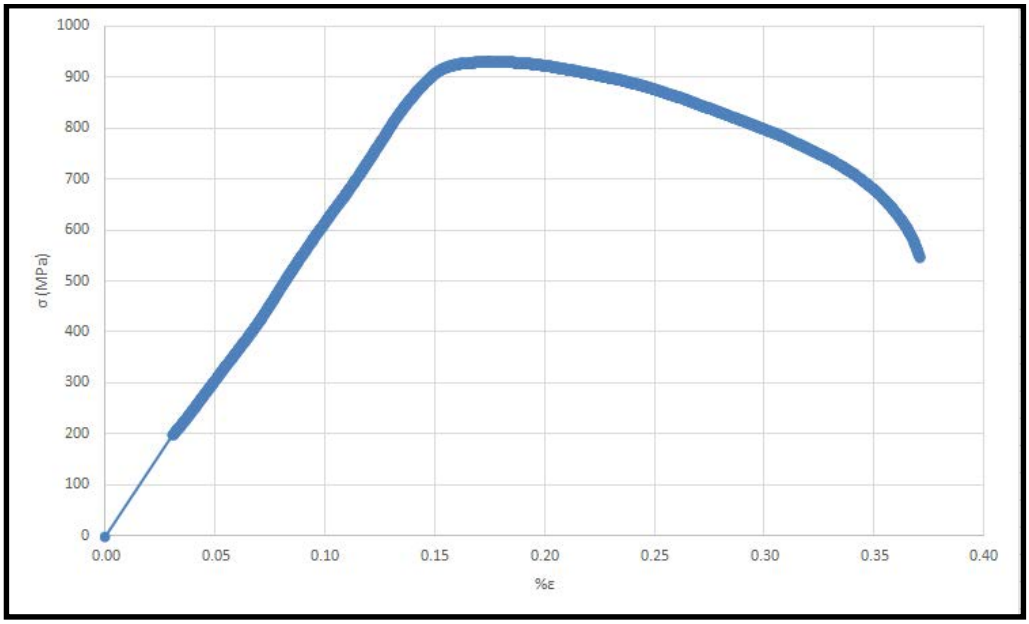

Figure D.3 ETN1 Stress-Strain Curve (Corrected)

10. REFERENCES

American Society for Metals (ASM). (1994). *ASM Handbook: Surface Engineering.* In S. R. Lampman (Ed.), Vol. 5. Ohio: ASM.

American Society for Testing and Materials (ASTM). (2009). E1558-09 Standard Guide for Electrolytic Polishing of Metallographic Specimens. West Conshohocken, PA.

ASM. (1964). *Metals Handbook* (8th ed., Vol. 2). Ohio: ASM.

ASM. (1973). *Metals Handbook* (8th ed., Vol. 8). Ohio: ASM.

ASM. (1990). ASM Handbook - Volume 1, Properties and Selection: Irons, Steels, and High-Performance Alloys.

ASTM. (2012). A370 Standard Test Methods and Definitions for Mechanical Testing of Steel Products.

Bernstein, I.M., & Thompson, W. (1986). Hydrogen Embrittlement of Steels. In M. B. Bever (Ed.). In *The encyclopedia of Materials Science and Engineering* (Vol. 3, pp. 2241-2245). Cambridge, Massachusetts: The MIT Press.

Bufalini, A. (2010). Preliminary Evaluation of Material for Expandable Applications According to the "Quick Assessment" Test Procedure. *Italy: Centro Sviluppo Materiali S.p.A.*

Busenberg, G.J. (2011). The policy dynamics of the trans-Alaska pipeline system. *Review of Policy Research (28:5).*

Caballero, F., Garcia-Junceda, A., Capdevila, C. & Garcia de Andres, C. (2006). Evolution of Microstructural Banding During the Manufacturing Process of Dual Phase Steels. *Materials Transactions, 47(9),* 2269-2276.

Courtney, T. H. (2000). *Mechanical Behavior of Materials*. United States of America: Waveland Press, Inc.

Fukuzawa, Y, Kojima, Y., Sekiguchi, E. & Mohori, N. (1993). Surface Modification of Stainless Steel by Electrical Discharge Machining. *ISIJ International, 33(9)*, 996-1002.

Herring, D.H. (2013). Segregation and Banding in Carbon and Alloy Steel. *The International Journal of Thermal Technology, Industrial Heating.*

Huang, X.P., & Cui, W.C. (2006). Effect of Bauschinger Effect and Yield Criterion on Residual Stress Distribution of Autofrettaged Tube. *Journal of Pressure Vessel Technology, 128*.

Jin, C.W., Wang, L., & Zhang, Y. (2012). Strength differential effect and influence of strength criterion on burse pressure of thin-walled pipelines. *Applied Mathematics and Mechanics (English Edition), 33(11).* 1361-1370.

Khanra, A., Pathak, L.C., & Godkhindi, M.M. (2007). Microanalysis of Debris Formed During Electrical Discharge Machining (EDM). *Journal of Material Science (42),* 872-877.

Kurtz, R.S. (2011). Oil Pipeline Regulation, Culture, and Integrity: The 2006 BP North Slope Spill. *Public Integrity, Winter 2010-2011 (13:1).* 25-40.

Latifi, A., Imani, M., Khorasani, M. T., & Joupari, M.D. (2013). Electrochemical and chemical methods for improving surface characteristics of 316L stainless steel for biomedical applications. *Surface & Coatings Technology, 221,* 12.

Li, C. C., Flasck, J.D., Yaker, J.A., & Leslie, W.C. (1977). On Minimizing the Bauschinger Effect in Steels by Dynamic Strain Aging. *Metallurgical Transactions A, 9A*.

Mack, R., Filippov, A., Kendziora, L., & Ring, L. (2000). In-Situ Expansion of Casing and Tubing - Effect on Mechanical Properties and Resistance to Sulfide Stress Cracking. *Corrosion, NACE International.*

Mack, R. & Filippov, A. (2002). The Effects of Cold Work and Strain Aging on the Hardness of Selected Grades of OCTG and on the SSC Resistance of SPI P-110. *Corrosion, NACE International.*

Mack, R. & Filippov, A. (2003). The Effect of Cold Work and Strain Aging on the Sulfide Stress Cracking Resistance and Mechanical Properties of Expanded Tubular Steels - A Laboratory Study. *Corrosion, NACE International*.

Meier, K, Kraemer, F & Wolter, K.J. (2012) *High Strain Rate Behaviour of Lead-Free Solders Depending on Alloy Composition and Thermal Aging.* IEEE.

Mishra, R.S., Sharma, S.R., Mara, N.A., & Mahoney, M.W. (2000). Mechanical Properties of Friction Stir Welded Aluminum Alloys. *Proceedings from Joining of Advanced and Specialty Materials,* St. Louis, MO, ASM International.

Ramasawmy, H & Blunt, L. (2007). Investigation of the Effect of Electrochemical Polishing on EDM Surfaces. *International Journal of Advanced Manufacturing Technology (31),* 1135-1147.

Sergueeva, A. V., Zhou, J., Meacham, B.E., & Branagan, D.J. (2009). Gage length and sample size effect on measured properties during tensile testing. *Materials Science and Engineering A, 516,* 4.

Zhu, X. & Leis, B.N. (2006). Average shear stress yield criterion and its application to plastic collapse analysis of pipelines. *International Journal of Pressure Vessels and Piping 83.* 663-671.

Zhu, X. & Leis, B.N. (2012). Evaluation of burse pressure prediction models for line pipes. *International Journal of Pressure Vessels and Piping 89.* 85-97.